UNIVERSIDAD AUTÓNOMA DE NUEVO LEÓN

FACULTAD DE INGENIERÍA MECÁNICA Y ELÉCTRICA

TESIS

COPPER ANTIMONY SULFIDE THIN FILMS BY SPRAY PYROLYSIS FOR PHOTOVOLTAIC APPLICATIONS

POR

JOSÉ AGUSTÍN AQUINO RAMOS

EN OPCIÓN AL GRADO DE

MAESTRÍA EN CIENCIAS DE LA INGENIERÍA MECÁNICA CON ESPECIALIDAD EN MATERIALES

MAYO, 2017

UNIVERSIDAD AUTÓNOMA DE NUEVO LEÓN

FACULTAD DE INGENIERÍA MECÁNICA Y ELÉCTRICA

SUBDIRECCIÓN DE ESTUDIOS DE POSGRADO

TESIS

COPPER ANTIMONY SULFIDE THIN FILMS BY SPRAY PYROLYSIS FOR PHOTOVOLTAIC APPLICATIONS

POR

JOSÉ AGUSTÍN AQUINO RAMOS

EN OPCIÓN AL GRADO DE

MAESTRÍA EN CIENCIAS DE LA INGENIERÍA MECÁNICA CON ESPECIALIDAD EN MATERIALES

SAN NICOLÁS DE LOS GARZA, NUEVO LEÓN, MÉXICO, MAYO, 2017

UNIVERSIDAD AUTÓNOMA DE NUEVO LEÓN

FACULTAD DE INGENIERÍA MECÁNICA Y ELÉCTRICA

SUBDIRECCIÓN DE ESTUDIOS DE POSGRADO

Los miembros del Comité recomendamos que la tesis "**Copper Antimony Sulfide Thin Films by Spray Pyrolysis for Photovoltaic Applications**", realizada por el alumno "José Agustín Aquino Ramos", con número de matrícula 1433769, sea aceptada para su defensa como opción al grado de "Maestría en Ciencias de la Ingeniería Mecánica con Especialidad en Materiales".

EL COMITÉ DE TESIS

DRA. BINDU KRISHNAN
DIRECTOR

DR. DAVID AVELLANEDA AVELLANEDA
REVISOR

DRA.SHADAI LUGO LOREDO
REVISOR

DR. SIMÓN MARTÍNEZ MARTÍNEZ
SUBDIRECTOR DE ESTUDIOS DE POSGRADO

San Nicolás de los Garza, Nuevo León, a mayo de 2017

Dedicatory

To my mother Dr. Patricia Danahe Ramos López for her constant support and example at all times, she demads herself every day to give her best. To be a excellent doctor, a responsible teacher, and a great mom. Who is the person I most want, and for her I am,thank you cute mommy.

Acknowledgments

For this research work, although it takes my name for defense, it is also part of all the people and institutions that trusted and supported me during this stage.

Dr. Bindu Krishnan: For the opportunity of working in this research project, her support with the reagents and the laboratory equipment for the experimentation. For her time and knowledge brought to be a researcher.

Dr. David Avellaneda Avellaneda: For his advice, his thesis review, his support and his time granted for the characterization with the XPS.

Dr. Shadai Lugo Loredo: For her advice, and her review for the thesis.

Dr. Sadasivan Shaji: For characterized by AFM the thin films and the observations during the master.

UANL: To my *alma mater*, for being a source of knowledge and culture, allowing me to develop my skills and give me a professional training to meet the challenges of our society.

CONACYT: To the National Science and Technology Council for the scholarship granted during the master's degree.

CIIDIT: For being my great working place during this research. To all the staff, for gave me an excellent attention during my stay.

FIME-CIDET: For the access to the laboratories and the equipment for the characterization of the thin films.

IER-UNAM: For characterized by GIXRD the thin films.

FCQ-Postgraduate: For the access to the Stylus Profiles for my characterization of thin films.

MSc. Pedro Martín Várguez: For his teaches of chemistry topics, and for showing me LaTeX as a more complicated way of writing a thesis.

MSc. Daniel Acuña Leal: For his observations of the physics topics, and more important for being a permanent member of the coffee club.

Contents

Abstract

The present project is on the synthesis of absorber material which belongs to I-V-VI group viz Copper Antimony Sulfide thin films by spray pyrolysis technique. $CuSbS_2$ has an ideal optical band gap of E_g=1.55 eV [1] that is suitable for photovoltaic applications. The spray pyrolysis technique is a chemical deposition that it does not need vacuum and also the process is carried at low temperatures near 500 °C. We obtained good quality thin films of thickness under $1\mu m$ using this low cost technique.

In chapter one, Thin Film Solar Cells, it is mentioned how the first photovoltaic cell was born, and the theory of the Photovoltaic effect. It was shown the functionally of a typical pn junction solar cell, the PV structures and the configurations used in the photovoltaic industry.

In chapter two, $CuSbS_2$: a novel photovoltaic material, a summary on different types of deposition techniques for thin films is presented. Further, a detailed description on the spray pyrolysis method along with a complete theoretical views on the mechanism of the film growth process.

Chapter three, Experimentation, begins with the problem approach, the justification of the present study, the objectives, and the proposed hypothesis. The chapter continues with the approach of experiments through a diagram of the prototype spray pyrolysis set up and the parameters that were considered for the synthesis process. Further, description of the characterization technique used for

the present work are given. In chapter four, Characterization of $CuSbS_2$ thin films, detailed analysis of the results is presented.

In chapter five, Conclusions and recommendations, the important findings of the present research project are highlighted and also, further scope of the project.

1 Thin Film Solar Cells

"There's plenty of room at the bottom."

by Richard Phillips Feynman.

1.1 Introduction

The key factors to slow down the development of the photovoltaic industry in its early days were the costs of production, the availability of raw materials, the toxicity of the materials during manufacture [2] and the competition against oil industry. At that point, a new technology based on the silicon wafer has had an important role in this technology for the development. Considering the thickness necessary for the fabrication of a monocrystal solar cell between 250 µm to 300 µm implied a high cost of production [3]. In this way, the raw materials and the Czochralski process reflect in a 50% of the total module cost [4]. So it has had an interest to reduce the thickness of the material without decreasing the efficiency, with this Thin Film technology, the reduction of the material cost and thus production of a solar cell would be profitable [5].

There are a few specific definitions for thin films. Some of them refer to the thickness and others to how the layers are formed. Focusing on the layer growth view, formation of thin film depending on condensation or nucleation or ionic reaction of species (atoms/moleculas/ions) on the surface substrate (metal, polymer

or glass) as homogeneous solid material that can be single crystalline, polycrystalline, or amorphous structure [3, 6, 7].

In addition to the cost benefit, there are other reasons for interests in thin films. Some of them are the following: facility to use any substrate shapes for growth thin film, monolithic integration between others thin films, facility of large areas for growth thin film, the availability of numerous deposition techniques, different configurations of the junctions for the cells, complementary films for a range of bandgaps, deposition parameters control to improve the film properties and the reagent reduction in the synthesis, short payback to the costumer, synthesis at low temperature, and ability of forming of transparent modules for buildings and homes [3, 5].

Thus thin films have a special attention in the photovoltaic research and development. Also, the proper use of the resources are indeed for viable manufacture with a low impact in the environment [2].

1.1.1 Semiconducting Thin Films

The compound semiconductors are the compounds between different groups of elements, to form new thin film materials in configurations as binary, ternary and quaternary having a specifics lattice constants, bandgap values, and index refraction for specific applications.

The group elements define the properties of the solid materials and the kind of crystal structure [5].

The semiconductor at absolute zero kelvin acts as an insulator and has high energy gap (E_g) between the valence band and the conduction band.

The valence band is a lower energy band that is occupied by valence electrons and the conduction band is an upper energy band where the conduction of electrons generate the current. The semiconductor conductivity is between the metal conductivity and insulator conductivity, which is conditioned by E_g. Example, some semiconductor with an extremely small E_g could be the InAs, with a

$E_g = 0.36eV$, compared of the $E_g = 2.42eV$ of CdS [5, 8, 9].

The electrical conductivity (σ) is the inverse of the resistivity (ρ) of a material. From the Ohm's law, (σ) is equal of current density (J) divided by electric field strength ($\mathscr{E}$) as is showed in **Eq.** (1.1).

$$\sigma = \frac{J}{\mathscr{E}} \tag{1.1}$$

With current density equals as $J = \mathscr{N}\mathscr{V}q_e$ and the electric field equals as $\mathscr{E} = \frac{\mathscr{V}m_e}{\tau q_e}$.

Then, the conductivity in a semiconductor is given by the **Eq.** (1.2).

$$\sigma = \frac{\mathscr{N}{q_e}^2\tau}{m_e} \tag{1.2}$$

Where: τ is the relaxation time, $\mathscr{N}$ is the number of electrons, $\mathscr{V}$ is the drift velocity, q_e is the charge of electron, and m_e is the mass of electron.

Other factors which impact the semiconductor properties are the intrinsic defects that contribute to conduction. The intrinsic defects belong to the crystal structure, that is why they are known as stoichiometric defects. The vacancy defect is called Schottky defect and the interstitial defect is Frenkel defect. The Schottky defects are cation and anion vacancies in a lattice with an overall neutral charge in the solid. The Frenkel defects are atoms or ions shifting at sublattice between unoccupied site in the crystal [10].

Apart from the intrinsics defects, most of the semiconductors used in the technology applications are fabricated with extrinsic defects. The extrinsic defects are the impurity aggregated in the crystals causing vacancies or excess of electrons. Thus both extrinsic and intrinsic defects can contribute n-type and p-type conductivity.

The n-type semiconductor present surplus of free electrons and the p-type present electron vacancies known as holes. In band theory, a hole represents an electron vacant state in a band and is dynamically considered as an electron of positive charge sited with a wave vector [8].

By bringing together a p-type and a n-type semiconductor, a junction is formed, this may be homojunction or heterojunction, which has the function of separating the charge carriers generated by the electromagnetic radiation (illumination) [5]. As seen in **Fig.** (1.1), a junction is formed between the same material as the p-type and the n-type semiconductor, it is said to be homojunction and thus has the same optical characteristics in the two semiconductors. This type of junction is manufactured using silicon (Si) as a material in the form of wafers, and is widely used in electronics and optoelectronics industry. When a union between different materials of p-type and n-type semiconductivity, it is said to be a heterojunction as shown in **Fig.** (1.1b). In the photovoltaic thin film technology, this configuration is used mostly, such as CdTe and CIGS based solar cells.

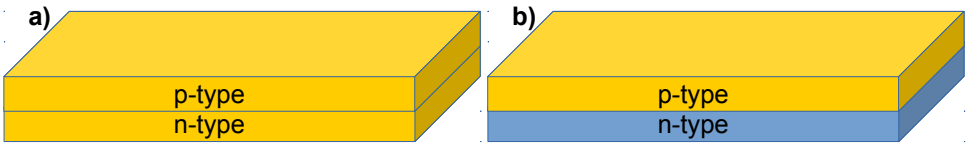

Figure 1.1: a) Homojunction has the same material in p-type and n-type. b) Heterojunction has different material between p-type and n-type.

Thin film solar cells basically are p-n heterojunction diodes, which can generate electric energy by photovoltaic effect when they are exposed to sunlight [5, 11, 12]. In this way, the energy generated in solar cell is due to photovoltaic effect, and it can explained using solar cell equation.

1.1.2 Solar cell equation

We already said the tremendous development in photovoltaic cells since Shockley *et al.* contributed. The first **Eq.** (1.3) represents a diode behavior.

$$I_D = I_0\left[exp\left(\frac{V + IR_s}{nV_T}\right) - 1\right] \tag{1.3}$$

And it is called Shockley diode equation, where:

I: is the current

I_{pv}: is the current generated by incidence of light.

I_0: is the reverse saturation current.

N_s: is the number of cells connected in series.

V_D is the voltage.

n: is the diode ideal factor.

V_T: is the thermal voltage.

The thermal voltage is represented with **Eq.** (1.4) [5].

$$V_T = \frac{k_B T}{q} \tag{1.4}$$

Where,

q: is the electron charge ($1.602\,166\,46 \times 10^{-19}$ C).

k_B: is the Boltzman constant ($1.380\,650\,3 \times 10^{-23}$ J/K).

T: is the temperature (K).

Starting from the Shockley diode equation there are three general approaches to represent a solar cell, these are the single diode model, the double diode, and the triple diode model [13, 14]. The single diode model is illustrated in the circuit diagram **Eq.** (1.2). It shows the current source parallel to the diode and it takes into account the shunt resistance (R_p) and series resistance (R_s).

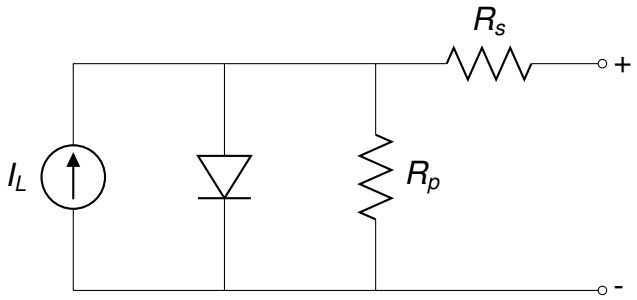

Figure 1.2: Circuit diagram of single diode model for solar cell

The mathematical interpretation is represented in **Eq.** (1.5),

$$I = I_{pv} - I_0 \left[exp\left(\frac{V + IR_s}{nV_T}\right) - 1 \right] - \left(\frac{V + IR_s}{R_p}\right) \tag{1.5}$$

Where R_s are the series resistances and R_p are the parallel resistances. Already in the field when a solar panel is working there are low efficiencies due the recombination loss in the depletion region that were not taken into consideration in the single diode model. For the double diode model these losses are considered. It shows the circuit diagram, where we can already see a second diode in parallel of the current source and the other diode in **Fig.** (1.3). The mathematic interpreta-

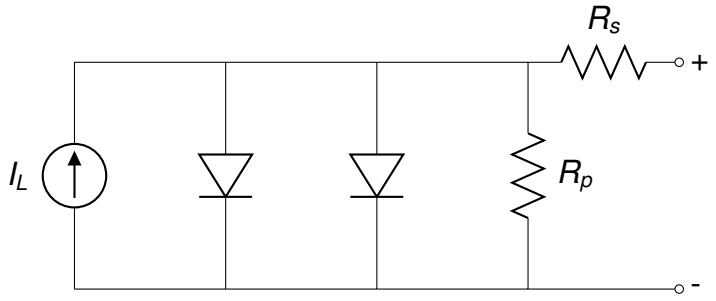

Figure 1.3: Circuit diagram of double diode model of solar cell

tion shows in **Eq.** (1.6), where it aggregates a second diode for the recombination loss in the depletion region. For the calculation used the Levenberg-Marquardt algorithm for solving curve fitting to obtain the I-V curves [15].

$$I = I_{pv} - I_{01}\left[exp\left(\frac{V + IR_s}{n_1 V_{T1}}\right) - 1\right] - I_{02}\left[exp\left(\frac{V + IR_s}{n_2 V_{T2}}\right) - 1\right] - \left(\frac{V + IR_s}{R_p}\right) \quad (1.6)$$

1.1.3 Inorganic thin films

The suitable properties of absorber thin films for photovoltaic application are:

1. The direct of bandgap of 1 eV to 1.5 eV.
2. The optic absorption coefficient is around of $1 \times 10^4\,\mathrm{cm}^{-1}$ to $1 \times 10^6\,\mathrm{cm}^{-1}$.
3. The conductivity of the material is $0.03\,\Omega^{-1}\,\mathrm{cm}^{-1}$ [16].
4. Low ratio or recombination velocity of charge carriers generated.
5. High diffusion length of charge carriers.

6. Materials abundance for large scale.

7. Non toxic and reproducibles fabrication.

So far, the main approaches thin film photovoltaics have been dominated by $a-Si:H$, CdTe, CIS & CIGS based Solar Cells [17].

Amorphous silicon ($a-Si:H$) Photovoltaic Semiconductor

Being a highly investigated the technology of silicon thin films have gained the most attention by the photovoltaic industry. The $a-Si:H$ thin films are a kind of silicon technology with amorphous structure. Currently, the efficiency of $a-Si:H$ thin films are 13.6% in a triple junction by substrate configuration [18].

The material has two drawbacks, when exposed to sunlight undergoes a degradation effect of the material known as effect Staebler-Wronski and conversion efficiency is about half the efficiency of solar cells with silicon wafer [19]. A typical configurations of $a-Si:H$ thin films are show in **Fig.** (1.4).

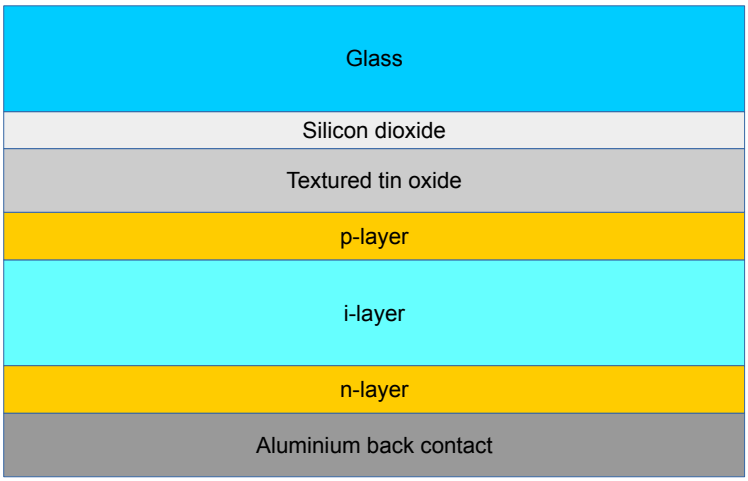

Figure 1.4: Schematic of solar cell based on a-Si:H [20].

CdTe Photovoltaics

Cadmium telluride thin films are used as an absorber material due to their ideal energy gap of 1.45 eV with direct absorption coefficient [21]. The efficiency of CdTe thin films have achieved 22.1% by First Solar [22].

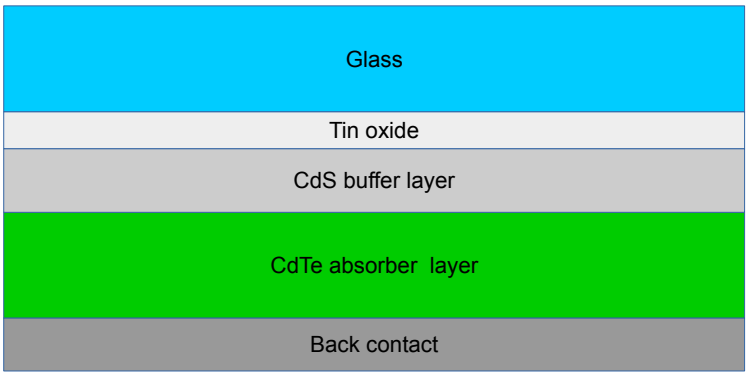

Figure 1.5: Schematic of CdTe solar cell based on [20].

The techniques usually used for the deposition of CdTe are closed space sublimation, physical deposit by evaporation, electro-deposition, chemical spray and electroplating. [3, 4].

Some drawbacks of such solar cells are the lack of research and development on CdTe thin films. One of the factor is the toxicity of cadmium in the environment during the life cycle of the thin films. Another issue is the degradation of the ohmic or the resistive contact [3, 4].

CIS & CIGS Photovoltaics

Copper indium sulfide or selenide (CIS) and copper indium gallium sulfide or selenide (CIGS) are materials containing elements of IB, IIIA and VIA groups of the periodic table, which possess high optical absorption coefficients. The best efficiency of CIGS thin film cell laboratory scale was 22.3 % by the company Solar Frontier [23]. The biggest problem of this technology is the scarcity of indium. $CuInS_2$ has a band gap of 1.53 eV of which is suitable as an absorber material. The research on thin films CIS and CIGS, lead to obtain a suitable bandgap to

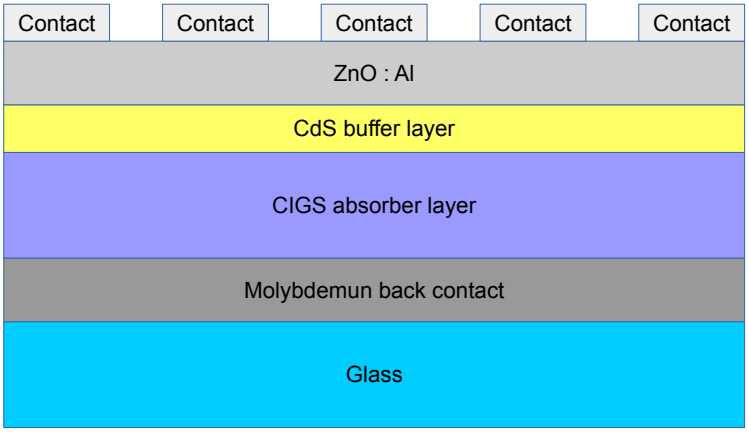

Figure 1.6: Schematic of CIGS solar cell based on [20].

achieve high efficiencies, the technology contains of alloying or $In_{1-x}Ga_x$. These cations to be present in the lattice prevent easy mobility of copper ions (Cu^+) so that the thin film is stable [16], and hence the device performance.

The elements involved at the fabrication of CIS and CIGS thin films increase the complexity of the processes, limiting the reproducibility, so it is important to have control of the stoichiometry during the deposition. The high price of In and Ga makes this technology costlier [3, 4].

1.1.4 New materials for Thin Film Photovoltaic

Perovskite

The Perovskite thin films have direct energy gap of 1.55 eV, and achieved 22.1 % efficiency in 2015 by KRICT/UNIST [24].

Much of the research on a global level in this new material called perovskites, in honor of Gustav Rose in 1839, are already of great interest in applications of optoelectronics because of its low cost of using organic compounds unlike those used in inorganic cells and because the manufacturing process. Perovskite has a crystal structure as calcium titanate with a general formula ABX_3, wich forms octahedral geometry (O_h and octahedral cube). It has twelve coordinated cations

Figure 1.7: Schematic of Perovskite solar cell based on [25].

(A, B) and six anions (X) [26,27], where A is the organic cation which are $CH_3NH_3^+$ or $NH_2CH_3NH_2^+$, and the other cation is the divalent metal Pb^{2+} or Sn^{2+}, and the anion is a monovalent halide which can be the (I^-,Br^-, Cl^-) [28].

For applications in solar cells it is used as absorber material between an electron carrier film and a holes carrier film, where at only nanometers thickness of deposition is sufficient [27].

CZTS

An absorber material known by its acronym (CZTS) is the quaternary semiconductor Cu_2ZnSnS_4, which has low toxicity, its raw materials are abundant. Recently, it has been reported the CZTS with an efficiency of 12.6% in laboratory cells using hydrazine based pure solution by spin coating [29].

Currently for this absorber material, there are many synthesis testings using diverse deposition techniques to develop a inexpensive production process. For example, the spray pyrolysis and sputtering [30]. This material is obtained by replacing in the ternary CIS, to indium (In) by 0.5 zinc(Zn) and 0.5 of tin(Sn) [30].

It has a direct band gap of 1.5 eV, with an absorption coefficient at visible region near $10^4\,cm^{-1}$ and shows a kesterite crystal structure [30]. As illustrated in **Fig.** (1.8), the usual configuration is a glass substrate, coated molybdenum (Mo),

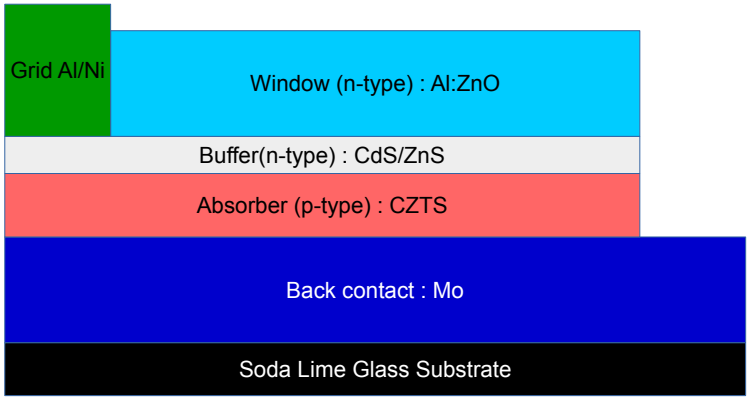

Figure 1.8: Schematic of solar cell based on CZTS [30].

absorber p-type material with CZTS, the material n-type CdS or ZnS, the window layer of zinc oxide doped with aluminum, and a contact of aluminum or nickel.

1.2 $CuSbS_2$ Thin Films

The cost of the production, the abundance of raw materials, and the high efficiency absorber properties lead the $CuSbS_2$ thin film to be innovate in this area. $CuSbS_2$ thin film has been reported in literature with a suitable bandgap around of E_g=1.52 eV [16, 31, 32] and it presents p-type conductivity of $2 \times 10^{-4}\,\Omega^{-1}\,\mathrm{cm}^{-1}$ [16].

Chalcostibite ($CuSbS_2$) is a compound semiconductor belongs to I-V-VI group and exhibits an orthorhombic crystal structure with a space group Pnma (No. 62) [16, 33, 34]. It can be observed a lead gray or gray iron color with metallic gloss [35] with lattice parameters a=6.018 Å, b=3.7958 Å, and c=14.495 Å [16, 33, 34]. The chemical composition (w/w %), corresponding atomic masses to obtaine the $CuSbS_2$ phase, are copper (25.48%), antimony (48.815%) and sulfur (25.71%) [16].

Cu, Sb and S are low toxic materials and abundant in the earth's crust [36] compared with the scarcity of In, Ga, and Te [37]. Among various techniques to

prepare thin films, spray pyrolysis has the features and the proven technologies in industries such as oil, automotive, and coatings parts.

1.2.1 Hypothesis

$CuSbS_2$ thin films of suitable PV properties can be synthesized by spray pyrolysis by varying the molar ratio of Cu, Sb and S in the precursor solution at varying substrate temperature.

1.2.2 General objective

To synthesize thin films of $CuSbS_2$ using the precursors of copper (Cu), antimony (Sb) and sulfur (S) in aqueous, aqueous-alcoholic or alcoholic solution by spray pyrolysis.

1.2.3 Specific objective

Specific objectives for this project were achieved as follows:

1. To refine spray pyrolysis set up.
2. To find a suitable molarity $S/(Cu + Sb)$ ratio in the precursor solution.
3. To obtain the optimum parameters of substrate temperature required for a homogeneous thin film of $CuSbS_2$.
4. To characterize the composition, morphology, crystalline structure, elemental compositions, and electrical/optical properties of the $CuSbS_2$ thin films.

2 $CuSbS_2$: a novel photovoltaic material

2.1 Structure and properties

The $CuSbS_2$ phase has its mineral name as chalcostibite, is one of the three phases, in the ternary system of copper antimony sulfide ternary known as Cu_3SbS_4 (Famatinite), Cu_3SbS_3 (Skinnerite / Wittichenite) and $Cu_{12}Sb_{14}S_{13}$ (Tetrahedrite) [38] and it is a compound semiconductor of I-V-VI groups according to the periodic table.

It can be observed in lead gray or gray iron color with metallic gloss in its appearance [35]. The mass density was reported as $4.95\,g\,cm^{-1}$ and the decay from ternary to binary is due to the low boiling point of sulfur at $444.6\,^{\circ}C$.

In the present study, the precursors used for the synthesis ($CuCl_2$, $SbCl_3$, NH_2CSNH_2) obey these conditions, in same way the solvents (H_2O, CH_3CH_2OH) and the air as transport carrier of the precursor solution.

There have been reported depositions of $CuSbS_2$ thin films by thermal evaporation, chemical bath, electrodeposition, and spin coating [39]. In addition, of to obtain the $CuSbS_2$ phase, it must be possible to have a scalable process for mass production. The spray pyrolysis technique has the features of scalability production as of thin films.

Crystal structure

It has a crystal structure of orthorhombic form as shown in **Fig.** (2.1) where its lattice parameters are a=6.018 Å, b=3.7958 Å, and c=14.495 Å; with traces of chlorine (Cl) and iron (Fe) from the Pnma space group and crystal system class number 62 corresponding to a bipyramidal as it has been reported in JCPDS 44-1417 and literature [16, 33, 34].

Its unit cell contains a total of sixteen atoms with four copper (Cu), four antimony (Sb) and eight sulfur (S) atoms. The layered structure can have some advantages such as the structural stability, better charge transport properties and the ability to form the interface structures comparing with other structural forms [40].

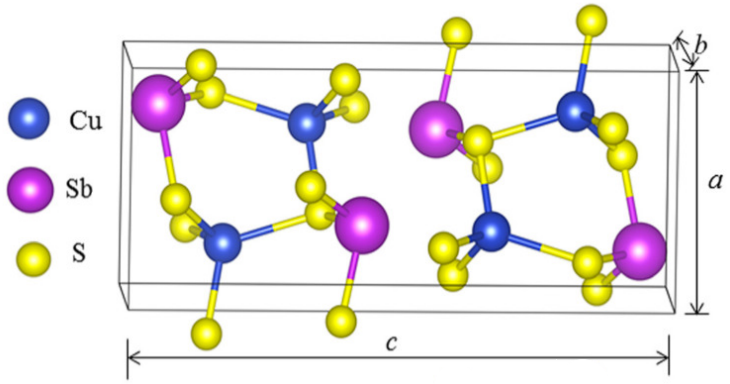

Figure 2.1: Orthorhombic structure of $CuSbS_2$ phase that shows a normal view of the unit cell [41]."Reprinted from [Mukesh Kumar and Clas Persson. $CuSbS_2$ and $CuBiS_2$ as potential absorber materials for thin-film solar cells. Journal of Renewable and Sustainable Energy, 5(3), 2013.] with the permission of AIP Publishing."

There were many studies reported of $CuSbS_2$ synthesize and its crystal structure. Since 2001, Rodriguez *et al.* reported that $CuSbS_2$ phase was synthesized in a range of 350 °C- 400 °C and they proved that chalcostibite phase was formed with X-ray diffraction and evaluated 20 nm cristallite size by Scherrer **Eq.** (4.1) [16]. Starting from 2008, Rabhi *et al.* deposited by thermal evaporation and annealed at

different temperatures. The samples below 200 °C, had amorphous phase while for the annealed samples exceeding 200 °C, they formed $CuSbS_2$ polycrystalline structures. Rodriguez *et al.* used the Scherrer **Eq.** (4.1) to determine crystallite size. From samples annealed at 200 °C, they reported 60 nm of diameter using the (200) plane and they observed that increasing the substrate temperature will decreased the bandgap [42, 43].

Electrical properties

The $CuSbS_2$ thin films exhibited p-type conductivity of $2 \times 10^{-4}\,\Omega^{-1}\,cm^{-1}$ by chemical bath deposition in thin films [16].

In theory simulation, phase stability and defects structure using first principles, it is found that $CuSbS_2$ phase possesses a p-type conductivity due to the shallow defect of copper vacancy (V_{cu}) with lowest formation energy in all electrochemical potential conditions [39].

Rodriguez *et al.* reported a resistivity of 35 Ω *cm* (dark) and under light a very low resistivity. In the test of hot probe obtained a $0.03\Omega^{-1}$ cm^{-1} and an p-type material [16].

Rabhi *et al.* presented resistivity of below 200 °C annealed samples values of 3.10^{-2} to 9.10^{-2} Ω cm and for samples annealed at 200 °C, they reported values of 2 Ω cm and the hot probe determined the p-type conductivity of their thin films [42, 44].

Optical properties

The $CuSbS_2$ thin film has been reported possess a bandgap of E_g=1.52 eV, suitable for pv applications [16, 31, 32]

The optical absorption spectrum and the optical band gap of this material were calculated theoretically by Lipping Yu *et al.*, their calculation showed an enhancement in absorption strength through the s-like valance band to p-like conduction band since Sb is in oxidation state of 3^+ (s^2 p^0 configuration) in this compound,

the absorption values were even higher than that of $CuInSe_2$ [45] as shown in **Fig.** (2.2). This is due to the sharp conduction band minimum (CBM) in contrary to the flat band nature of $CuInSe_2$. According to the calculations based on GW approximations for the electrons self energy, the absorption coefficient rises more that $10^5\ cm^{-1}$ above its band gap energy of 1.5 eV, which is the ideal band gap for the best photovoltaic conversion efficiency. Experimentally direct allowed transition across a band gap of 1.5 eV.

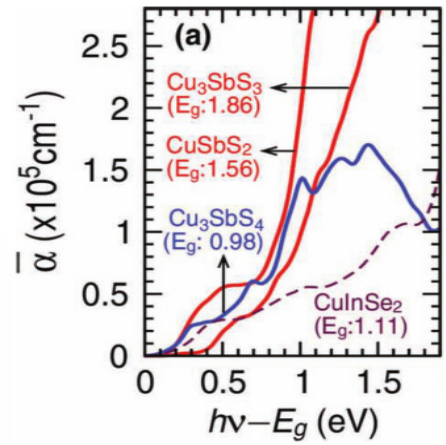

Figure 2.2: Calculated optical absorption spectra for $Cu-V^{5+}-VI$ compounds (blue) and $Cu-V^{3+}-VI$ compounds (red) [45]."Reprinted from [Liping Yu, Robert S. Kokenyesi, Douglas a. Keszler, and Alex Zunger. Inverse design of high absorption thin-film photovoltaic materials. Advanced Energy Materials, 3:43–48, 2013.] with the permission of John Wiley and Sons."

The $CuSbS_2$ semiconductor has a wide direct bandgap between 1.38 eV to 1.5 eV [16, 39]. The optical absorption coefficient over $10^4 cm^{-1}$ [39] is suitable for terrestrial solar cell. In the transmission of $CuSbS_2$ with a 900 nm of wavelength results with 50% of transmission, then the absorption coefficient (α) is obtained with **Eq.** (2.1), where d is the thickness, R is the reflectance, and T% is the transmittance data [46].

$$\alpha = \frac{1}{d} \ln\left(\frac{(1-R)^2}{T}\right) \tag{2.1}$$

Now, the bandgap can be calculated, through ($h\nu$) vs $(\alpha h\nu)^n$ plot, extrapolating the linear region to τ [45]. (α hv)^n relation shows in **Eq.** (2.2), where h is the Planck's

constant, A is a constant, v is frequency of the photon and n has a different values 2, 1/2, 3/2. For this case, $n = 2$ value due to direct bandgap reported for $CuSbS_2$ [47].

$$(\alpha hv)^n = A(hv - E_g) \tag{2.2}$$

2.2 Synthesis methods

There are different deposition techniques for thin films, we can classify into physical and chemical deposits. Different types of physical depositions as Laser ablation, Sputtering, Molecular beam epitaxy (MBE), and Physical vapor deposition (PVD) have been reported in the literature for thin films [48].

For the chemical deposition of thin films is divided into two types, gas phase reaction and solution phase reaction [48, 49]. Gas phase methods include chemical vapor deposition (CVD), and atomic layer epitaxy. For solution phase reaction include Spray Pyrolysis, Sol-Gel, centrifugal thin film, immersion thin film, and chemical bath deposition (CBD) [50].

$CuSbS_2$ thin films have been obtained by chemical bath deposition [16, 50], thermal vacuum evaporation [43, 51], electrodeposition [52–55], spin coating [39], hydrid of CBD & TVE [31, 46, 47], and spray pyrolysis [56–61], which will be briefly explained below.

2.2.1 Chemical bath deposition (CBD)

Chemical bath deposition is commonly used for thin films deposition due its simplicity, low cost, scalability and viability as its advantages compared to other techniques. There are basic chemical reagents used for the synthesis of $CuSbS_2$ thin films. They are antimony trichloride ($SbCl_3$), acetone ($(CH_3)_2CO$), sodium thiosulphate ($Na_2S_2O_3$), copper (II) chloride ($CuCl_2$) dimethylthiourea ($CH_3NHCSNHCH_3$) and water (H_2O) [16, 50].

There are two ways of chemical procesees to form $CuSbS_2$. One way, the deposition of Sb_2S_3 thin film and then the deposition on this one, the CuS followed by heating [16] as shown in **Table** 2.1.

Table 2.1: Two baths [16]

Step	Description
1	1^{st} bath preparation stirred continuously at 10 °C for 4 h: 5 mL of acetone + 1.3 g of $SbCl_3$ + 50 mL of 1*M* $Na_2S_2O_3$ at 10 °C + 145 mL of cold deionized water
2	50 mL of 1*M* $Na_2S_2O_3$ at 10 °C poured over of solution and stirred continuously.
3	145 mL of cold deionized water poured over the solution.
4	Glass substrates were placed vertically in the beaker bath and CBD was prepared at 10 °C for 4 h
5	Coated substrates were changed to a fresh bath by the same time. After, substrates were removed from the bath and rinsed with distilled water. Then, they were dried.
6	The 2^{nd} bath, 5 mL of 0.5 M $CuCl_2 \cdot 5\,H_2O$ mixed with 9 mL of 1 M $Na_2S_2O_3$ solution.
7	10 mL of 0.5 M dimethylthiourea were pour over and mixed to the solution.
8	79 mL distilled water was poured over the beaker.
9	Glass substrates were placed vertically in the beaker bath and CBD was prepared at 70 °C by 2 h.
10	Substrates were removed from the bath and rinsed with distilled water.Then they were dried.

Second method is the formation of the $CuSbS_2$ thin films from single bath containing (Cu), (Sb) and (S) sources [50].S.C.Ezugwu *et al.* prepared $CuSb_2S_2$ from chemical bath containing antimony trichloride ($SbCl_3$), acetone, sodium thiosulphate ($Na_2S_2O_3$), and copper (II) chloride ($CuCl_2$) as precursors for synthesis of $CuSbS_2$ thin films [50]. They synthesized as shown in **Table** (2.2).

2.2.2 Thermal Vacuum Evaporation(TVE)

Rabhi *et al.* prepared $CuSbS_2$ thin films on glass substrates by vacuum evaporation of $CuSbS_2$ powder, using heated molybdenum boats [42, 43]. The pressure

Table 2.2: One baths [50]

Step	Description
1	In 5 mL of acetone was added 1.3 g of $SbCl_3$
2	25 mL of 1M $Na_2S_2O_3$ poured over of solution.
3	5 mL of 0.1M $CuCl_2$ poured over the solution.
4	15 mL of H_2O poured over the solution.
5	Glass substrates immersed on the baker at 25 °C with four dip times(1 h, 1.5 h, 3 h, and 3.5 h).
6	Substrates were removed from the bath and rinsed with distilled water.Then they were dried

was at 10^{-5} Torr, in vacuum atmosphere for 2 h in a range of temperature of 130 °C to 200 °C.

Fadhli *et al.* deposited $CuSbS_2$ thin films by TVE at 100 °C onto glass substrates by 1 h. Then, they annealed at 250 °C for 60 min and 120 min the thin films [51].

2.2.3 Chemical bath deposition & thermal evaporation

C.Garza *et al.* formed in three processes the $CuSbS_2$ thin films, first a formation of Sb_2S_3 thin films by chemical bath deposition as described below. First process, on glass substrates by chemical bath deposition were made Sb_2S_3 thin films. To prepare the bath mixture the reactants: 1) 650 mg of $SbCl_3$ dissolved in 2.5 ml of acetone. 2) Added 25 ml of 1 M $Na_2S_2O_3$ pre-cooled. 3) Added 72.5 ml of deionized (pre-cooled) water. 4) Stirred well. 5) In a Petri dish placed in horizontal position the glass substrates (75 mm x 25 mm x 1 mm), then slowly pour the solution into the petri with a $t = 3h$ of deposition. Then in a vacuum of 10^{-5} *Torr* on a molybdenum boat a copper wire (99.99%) was evaporated on the glass/Sb_2S_3. With a in situ quartz crystal thickness monitor fixed as 20, 30, 40, and 50 nm. and third annealed the substrates to form the $CuSbS_2$ thin films [31]. Finally, Sb_2S_3 / Cu thin films were heated at 300 and 380 °C in vacuum of

10^{-3} *Torr* for 1 to 2 h [31].

R.E. Ornelas-Acosta *et al.* prepared Sb_2S_3 by chemical bath deposition like C.Garza *et al.* C.Garza *et al.* only added a second pathway, where the glass/Sb_2S_3/Cu thin films were annealed at 350 °C, 375 °C, 400 °C in low vacuum (10^{-3} Torr) for 1 h in a vacuum furnace [46, 47].

2.2.4 Electrodeposition

D. Colombara *et al.* deposited $CuSbS_2$ using precursor films of a molar ratio (1:1) of Cu:Sb by electrodeposition from aqueous solutions onto Mo coated glass substrates. In two configurations viz stacked and co-electroplated. In co-electroplated technique, they chose the thickness of 2 µm, and the temperature between 200 °C and 500 °C, for 5 to 960 min, and the heating rate between 5 and 600 °C min^{-1}. In a graphite box with elemental sulfur atmosphere the metal precursor films converted to the corresponding sulfides [52].

Ikeda *et al.* fabricated metallic stacks of Cu on Mo/glass substrate by electrodeposition won an aqueous solution containing 15 mmol dm^{-3} $CuSO_4$ and 15 mmol dm^{-3} citric acid at -0.4 V. After Cu-film deposited, an Sb film was deposited on the Cu/Mo/glass to an aqueous solution containing 15 mmol dm^{-3} $K_2(Sb_2(C_4H_2O_6)_2)$ and 50 mmol dm^{-3} tartaric acid at -0.3 V. With a fixed temperature at 24 °C by immersing the electrolyte solutions in a thermostatted water bath. The amount of deposited metal was estimated by the electric charge. In this study, metallic stacks with Cu/Sb atomic composition ratios. Thus obtained metallic stacks were sulfurized to form $CuSbS_2$ films using a three-step temperature profile. First, the precursor film was heated to 510 °C in Ar, and then heating at this temperature was continued for 60 min. In the second step, the film treated at 510 °C was cooled to 450 °C in Ar; sulfurization of the film was performed by introduction of hydrogen sulfide (H_2S, 5% in Ar) at this temperature for 30 min. Finally, the film was allowed to cool down to ambient temperature in Ar.

The XRD showed that the films were due rich in CuS, and $CuSbS_2$ phase. The formation temperature of $CuSbS_2$ was at 300 °C and the excess sulfur increase the formation of Sb_2S_3 [52].

Ikeda *et al.* did a water bath at 24±1 °C where they immersed an electrolyte cell of aqueous solution containing 15 mmol dm^{-3} of $CuSO_4$ as a precursor of Cu and 15 mmol dm^{-3} with citric acid ($C_6H_8O_7$) with a cell configuration of a three electrode cell where Mo/glass substrate like a working electrode, Pt wire as a counter electrode and an Ag/AgCl as a reference electrode. After the Cu thin film formation covering the Mo/glass substrate, the electrolyte solution changed for an aqueous solution containing 15 mmol dm^{-3} of $K_2(Sb_2(C_4H_2O_6)_2)$ and 50 mmol dm^{-3} of tartaric acid($C_4H_6O_6$) maintaining the 24±1 °C of the water bath. Finally a sulfurization with hydrogen sulfide in Ar atmosphere with a three step temperature profile(510-450- 25 °C) for 30 min [53].

Septina *et al.* reported that in water bath at 25 °C, they immersed an electrolyte cell of aqueous solution containing same parameters as Ikeda *et al.* [53], with pH adjusted to 1.3 by the addition of H_2SO_4, maintaining the 25 °C of the water bath. Finally a sulfurization with hydrogen sulfide in Ar atmosphere with a three step temperature profile (510-450-25 °C) for 30 min [54].

Rastogi *et al.* mixed 1 mol of choline chloride ($C_5H_{12}ONCl$) and 2 mol of urea ($(NH_2)_2CO$) at 80 °C under stirring. After, they obtained the Cu^{2+} from anhydrous salts $CuCl_2$ (99%) and the Sb^{3+} ions were derived from $SbCl_3$ (99%), with molar concentrations of Cu to Sb of 1:1; 1:1.4; and 1:0.71stoichiometric ratios. The sulfur ions were sourced by dissolving 10 mM sodium thiosulfate, $Na_2S_2O_3$ (99%) to the clear ChCl–urea solution containing $CuCl_2$ and $SbCl_3$ [55].

2.2.5 Spin coating

Yang *et al.* reported deposition by spin coating of 2 mL of hydrazine solution. They containing0.226 g of Cu and a 0.175 g of S. They stirred the solution for few days.

In parallel process, 2 mL of hydrazine were dissolved 0.484 g of Sb and a 0.445 g of S. It stirred for few days too. The two solutions were mixed with a Cu/Sb molar ratio of 0.9:1 and stirred t$\geq$ 2 h before deposition. On FTO substrates, the film was deposited by spin coating at 500 *rpm* for 10 s, and 2100 *rpm* for 45 s. Dried on a preheated blade at 100 °C for 10 min and then annealed at 250 °C by 3 min. Did by 4 times the spin coating deposition and the soft bake, then a final annealing at 350 °C for 10 min [39].

2.2.6 Spray pyrolysis thin films (SPTF)

The spray pyrolysis is a chemical deposition technique that was developed to deposit sulfides and selenides thin films.

In 1966, R.R. Chamberlin y J.S. Skarman published a deposition technique thin films sulfides and selenides, that was presented as the spray of solution on heated substrates, with the condition that the precurs elements were contained solely in the precursor solution to be sprayed [62].

Given the interest in the deposition of metals and oxides, J.C. Viguié and J. Spitz explained a chemical vapor deposition at temperature range $<$500 °C and a pressure of 100 *kPa*. It was described that the chemical reaction shall could be at low temperatures without vacuum. They classified four stages of the deposition mechanism at various substrate temperatures as shown in **Fig.** (2.3) [63].

A-Process: The drops are spread over the surface of substrate where the solvent is evaporated and the dried precipitate precursors decomposition takes place.

B-Process: The solvent is evaporated before falling the drops on the substrate surface, leaving a precipitate which decomposes on the substrate.

C-Process: The solvent evaporates from the drops nearby the substrate surface. The precipitated solids melt and sublime, and the vapor diffuses on the substrate by heterogeneous reaction.

D-Process: At high temperatures, the drops precipitate and sublime. A chemical reaction of precursors effect in vapor phase near the substrate surface.

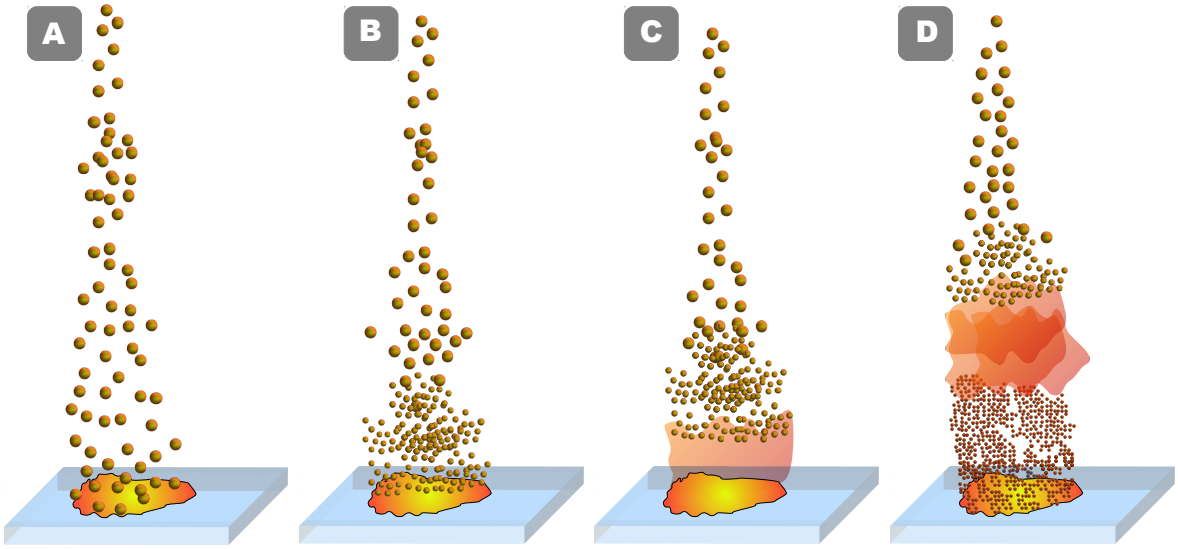

Figure 2.3: Deposition process with increasing substrate temperature. **(A)** The solvent is evaporated and the decomposition of dried precipitate precursors takes place. **(B)** The drops spread over substrate and the solvent is evaporated before the falling drops on the substrate surface, leaving a precipitate which decomposes on the substrate. **C:** The solvent evaporate at the drop nearby on the substrate surface. The precipitated solids melt and sublime, the vapor diffuse in the substrate in a heterogeneous reaction. **D:** At high temperatures, the drops precipitate and sublimate. A chemical reaction of precursors effect in vapor phase near the substrate surface [63].

Spray pyrolysis is used due this does not require vacuum, cost efficient, coatings complex geometry, high quality layers, uniformity of film, and scalability.

By spray pyrolysis technique, it can be synthesize dense and porous deposits films, with controlled thicknesses. It is also one of the preferred techniques for making powders and ceramic coatings [64].

The basic parts that constitute the spray pyrolysis equipment are the precursor solution container, the substrate heater, the spray nozzle, and the temperature controller. The spray pyrolysis technique was first used in 1966 by Chamberlin and Skarman to deposit CdS films for photovoltaic applications. The feasibility and scalability of this technique due to its reproducibility in the process and easiness for depositing noble metals, metal oxides, spinel oxides, chalcogenides and superconductor compounds, place it as a preferred technique over many other [65].

Theoretical aspect

The process of depositing thin films by spray pyrolysis includes many physical and chemical phenomena, and to date only been reported approaches for film formation. The entire process generally is divided into three stages, starting with the preparation of the solution, atomization of the solution, transportation of the atomized solution, to the hot substrate, decomposition of precursors and nucleation of the film on the substrates.

In the preparation of the precursor solution, care should be taken to choose precursors from the source elements to form the thin film, and a suitable solvent to dissolve the precursor solutes.

The parameters affect the growth, the morphology, and the properties of the thin films are atomization, aerosol transport, decomposition, substrate surface temperature, precursor solution and substrate-nozzle distance.

1. Atomization: The atomization of the precursor solution is a very important in making the type of spray that was used partly because depending on the application the ideal atomizer is adjusted. There are several types of atomizers, such as the air blast, ultrasonic, and electrostatic. In a study electrostatic atomizers stability have the load drops isolated with Rayleigth study, depending on the parameters of dew, there are different types of behavior of the solution was atomized. Currently, there are different atomizers where it can obtain a

various types of droplets and distributions. As examples there are the cone-jet, multi-jet, plane-jet, and dona-jet [48].

2. Aerosol transport: During aerosol transport process, the droplets travel from nozzle to substrate surface. Where they travel as liquid phase or they could change to a gas phase by the heat radiation near the substrate surface. There are forces those affect the trajectory and the evaporation of the droplets, these forces are the gravitational, electric, thermophoretic and Stokes [48].

3. Decomposition: The precursor droplets carry out a chemical reaction almost since it is close to the substrate surface, during spreads and after that. Viguie and Spitz observed this process with detail, and they proposed four process those can be occur [48, 63] as showing in the **Fig.** (2.3).

4. Substrate surface temperature: The temperature in surface substrate defines the morphology, the structure, and the properties of the thin films formed. In morphology, it was reported that the films had changed from dense to highly porous surface [48]. Also, for the films structure, it was observed that certain preferential plane orientation appeared in a direct relation with the film thickness. The optical and electrical properties are effected by the homogeneity of the film, that it influenced by temperature [48]. Due it takes part in the solvent evaporation process, it affects the droplets those impacted onto substrate surface, and it changes the precuror solution in the chemical reaction or the precursor decomposition, so it is an important parameter in the spray pyrolysis [48].

5. Precursor solution: It is the mixture of the solutes (salts), the solvent and in some cases additives, where it can varying the molar ratio of them for pursuit specifics properties and structures due they affect the chemical and physical properties of the precursor solution [48].

6. Substrate-Nozzle distance: The nozzle distance is defined by the manufacturers. The manufacturers design and test nozzles with a specif distance range functional to work. The substrate-nozzle distance, it is known as spray distance. It is search the theoretical coverage on the substrate surface, and this depends of the spray distance, the spray angle, the

viscosity of precursor solution, nozzle capacity and spraying pressure (Http://www.spray.com/cat76/automatic-m/offline/download.pdf, 16) [66].

State of art

S. Manolache *et al.* prepared $CuSbS_2$ thin films by spray pyrolysis on two types of substrates: First on TCO substrates, and second on TCO/dense TiO_2/nanoporous TiO_2 substrates. They used copper(II) chloride dehydrate($CuCl_2 \cdot 2\,H_2O$), antimony(III) acetate ($(CH_3COO)_3Sb$, thiourea (H_2NCSNH_2) as precursors of $CuSbS_2$ thin films, in aqueous solution with small amounts of HCl. The temperature was optimized at 240 °C with a carrier gas Argon (Ar), 1.2 bars of pressure, and at 27 cm of distance between fixed nozzle and heater [56–58].

I. Popovici *et al.* reported the formation of $CuSbS_2$ thin films with different molar ratios as showed in **Table** (2.3), on a FTO conductive glass substrates heated by sprayed with an aqueous solution of copper (II)-chloride dehydrate (Scharlau, $CuCl_2 \cdot 2\,H_2O$, min 99 %), antimony (III) acetate (Alfa Aesar, $(CH_3COO)_3Sb$, 99.99%), thiourea ($H_2NCSNH_2$99 % and the same S. Manolache *et al.*, they added few drops of HCl. The innovation in this synthesis, was that they added 100 ppm sodium maleate-methyl metacrylate (Hydrophilic polymer, HFL) and in other sample, added 100 ppm sodium maleate-vinyl acetate (hydrophobic polymer, HFB). At temperature of 240 °C, carrier gas (air) with pressure of 1.5 bar and distance of between nozzle and substrates of 25 cm, and pause of 60 seconds between two sprayed sequences [59]. They observed that increasing antimony in the precursor solution affect the grain size and the band gap increase.

Thiruvenkadam *et al.* prepared the precursor solution at 0.01 M of $CuCl_2$, 0.003 M (to 0.03 M in steps of 0.006 M) of $Sb(CH_3CO_2)_3$, 0.006 M of $SC(NH_2)_2$, and small amount of acetic acid in a aqueous solution. In the sprayed rate was at 5 mL min^{-1} onto a glass substrate at 240 °C to 320 °C with increase of 20 °C [60, 61].

Sample #	*Cu* : *Sb* : *S* (*molar ratio*)	Sample #	*Cu* : *Sb* : *S* (*molar ratio*)
A	1:1.48:13	E	1:4.4:13
B	1:1.97:13	F	1:1.84:13
C	1:2.48:13	G	1:1.84:13
D	1:3.47:13	H	1:1.84:13

Table 2.3: Precursor solution composition [59].

3 Experimentation

3.1 Introduction

In the literature there are only a few articles for copper antimony sulfide synthesis by spray pyrolysis; From the reports of Manolache *et al.*, they used argon as carrier gas [56–58], in that way, we preferred air due to its lower cost than argon. Other issue, as Manolache *et al.* and Popovici *et al.* reported the use of HCl for their synthesis to increase the solubility of the precursors [56–59]. Thiruvenkadam *et al.* used acetic acid for the precursor solubility [60, 61].

Based on the reports, we designed the experimental conditions of CuS as A product, Sb_2S_3 as B product, $CuSbS_2$ as C and D product formulation. The A product or CuS, to achieve the experience in the synthesis and deposition of binary thin films by spray pyrolysis technique. The B product or antimony sulfide thin films, it started to recycle the precursors from bath depositions, where the Sb_2S_3 nanoparticles were obtained by laser ablation from tablets of chemical bath wastes. The C and D products were the main synthesis of this research, the difference between them was that in the C-product, antimony(III) acetate was used as precursor for antimony and in D-product was used $SbCl_3$ as antimony precursor. The copper and sulfur precursors were the same for both products. In **Fig.** (3.1) shows a flow chart of the experimentation design to synthesize CuS, Sb_2S_3, and $CuSbS_2$ thin films.

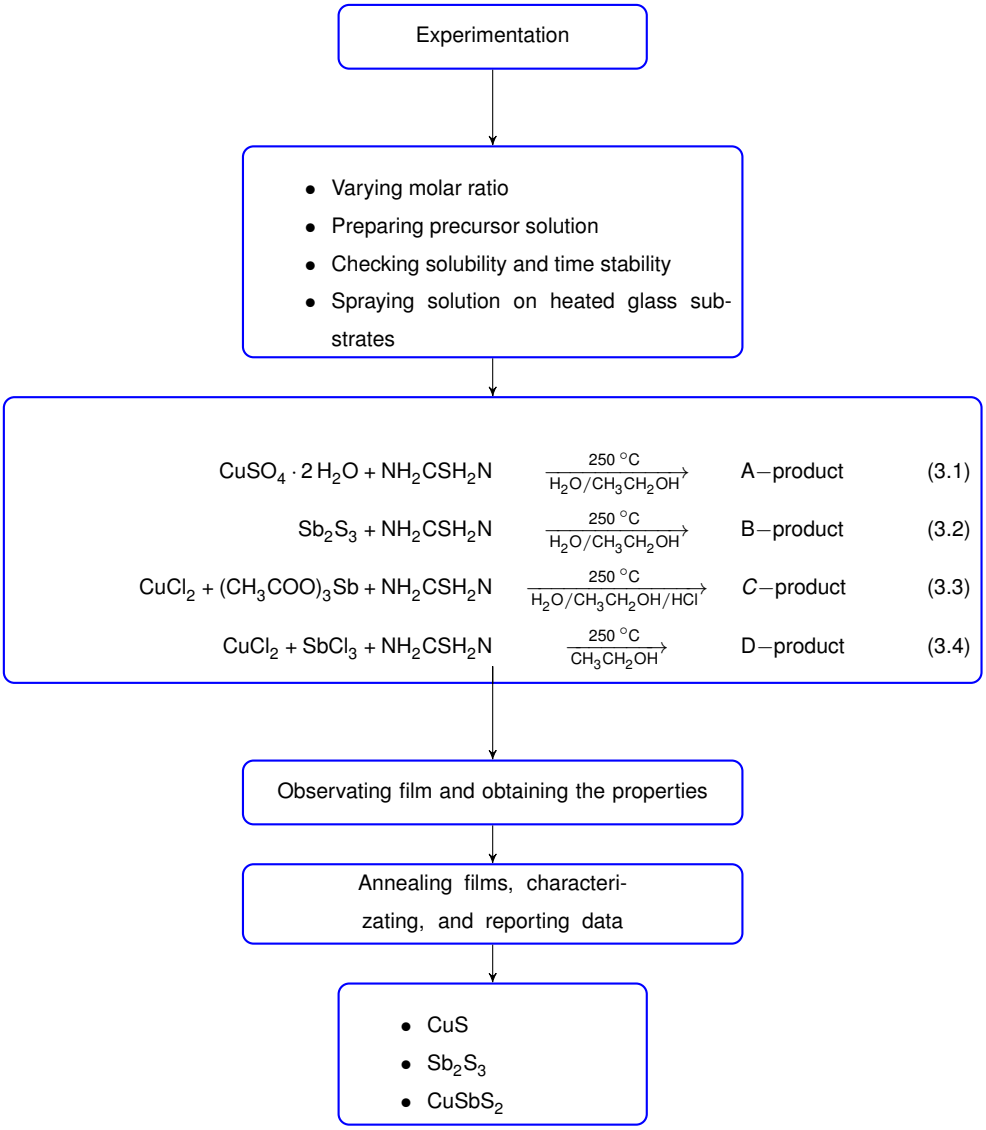

Figure 3.1: Experimental chart

3.2 Materials

3.2.1 Reactants

The aim was to prepare a low-cost synthesis for $CuSbS_2$ thin films, thus, low temperatures and inexpensive materials were preferred. The ethanol was chosen as solvent due to its high volatility.

The $SbCl_3$ was used as precursor of antimony based on a report of 2001 for Sb_2S_3 thin films by chemical bath deposition [16]. The used of $CuSO_4 \cdot 5\,H_2O$ was reported for coppper sulfide hollow spheres by hydrothermal conditions [67]. For the $CuSbS_2$ thin films synthesis by spray pyrolysis it was reported the use of $(CH_3COO)_3Sb$ as a precursor for antimony too, but by adding HCl to increase its water solubility [56–58]. The $CuCl_2$ was used as a precursor of copper for $CuSbS_2$ thin films by chemical bath deposition as reported by Ezugwu *et al.* [68], although it could also be $CuCl_2 \cdot 2\,H_2O$ as a precursor as reported by Manolache *et al.* [56–58].

Even when $Na_2S_2O_3$ has been employed in chemical bath deposition of $CuSbS_2$ [16], the H_2NCSNH_2 was preferred as precursor for the sulfur, because the decomposed species are volatile [56–58]. These materials are shown in **Table** (3.1).

The synthesis of copper sulfide precursor solution was made with $CuSO_4 \cdot 5\,H_2O$, NH_2CSH_2N, and deionized water. For the synthesis of antimony sulfide, the precursor solution was made with Sb_2S_3 nanoparticles, NH_2CSH_2N, and deionized water.

Synthesis $CuSbS_2$ was done with two different precursor solutions. The first precursor solution set was prepared by dissolution of $CuCl_2$, $(CH_3COO)_3Sb$, and NH_2CSH_2N in deionized water, CH_3CH_2OH, HCl, and HNO_3. The second precursor solution set was prepared with $CuCl_2$, $SbCl_3$, NH_2CSH_2N, deionized water and CH_3CH_2OH.

Table 3.1: Materials for experiments.

Formula	Assay	Name	Brand
$SbCl_3$	$\geq$ 99%	Antimony(III) chloride	Sigma-Aldrich
$CuCl_2$	99%	Copper(II) chloride, anhydrous	Acros Organics
NH_2CSH_2N	99%	Thiourea	Fermont
$(CH_3COO)_3Sb$	99.99%	Antimony (III) acetate	Aldrich
$CuSO_4 \cdot 5\,H_2O$	$\geq$98%	Copper(II) sulfate pentahydrate	Meyer
HCl	34 - 36%	Hydrochloric acid	Fermont
CH_3CH_2OH	99.7%	Ethanol	Fermont
H_2O	-	Deionized water	-

3.2.2 Spray Pyrolysis equipment

The spray pyrolysis equipment consisted of the following parts as shows in the **Fig.** (3.2).

- Laboratory extractor hood
- Pneumatic valve
- Air nozzle # 1
- Pneumatic push-in fittings
- Rigid hose
- Flexible hose
- Separation funnel valve
- Step motor
- Micro limit switch roller lever arm
- Heater

Spray pyrolysis procedure

We set two distances, between nozzle and heater at 25 cm and distance between micro limit switches for linear movement of the nozzle at 32 cm.

1. Set at 25 cm distance between nozzle and heater.
2. Set at 32 cm distance between micro limit switches.
3. Placed the cleaned substrates on the heater plate's surface.
4. Set the heater at 250 °C.
5. Pour the precursor solution in the 500 mL separatory funnel.

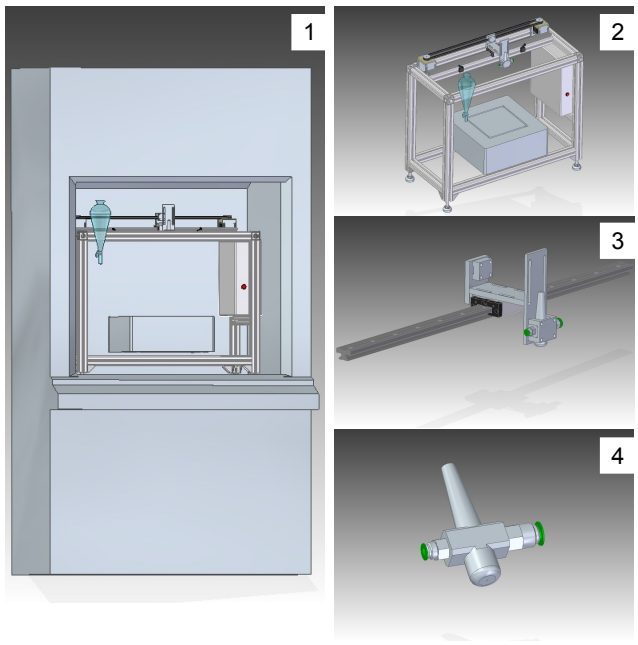

Figure 3.2: 1) General view of the spray pyrolysis equipment. 2) Zoom of the prototype of the spray pyrolysis. 3) The movement parts of the spray. 4) The stainless steel air nozzle.

6. To set the air pressure at 30 psi.

3.2.3 Substrate cleaning

Glass substrates (Corning®, 25 mm x 75 mm x 1mm) were used for the deposit. The substrates were contaminated with dusties/fuzzies and oil. It was reported in literature that cleaning process of substrate affect the reproducibility of the films [69]. The glass substrates were immersed in deionized water with liquid neutral detergent (Jalmek®). Then we carved with a flannel to remove completely the oil or dusty. After the substrates were rinsed of first with deionized water and then with isopropyl alcohol. Finally, we dried them in hot air.

3.3 Synthesis of Copper sulfide

Stock solution of $CuSO_4 \cdot 5\,H_2O$ at (1 M) concentration in 100 mL of Deionized water (DI water) was prepared. The molar mass of $CuSO_4 \cdot 5\,H_2O$ is 249.68 g mol^{-1} as solute. Where 1 M = 1 mol L^{-1} and 100 mL = 0.1 L. The $CuSO_4 \cdot 5\,H_2O$ mass needed was calculated multiplying volume $\times$ Molar Concentration $\times$ Molar Mass.
$(0.1\text{L})(1\text{mol L}^{-1})(249.68\text{g mol}^{-1})$ = 24.97g
Then, 24.97 g of $CuSO_4 \cdot 5\,H_2O$ were dissolved in 100 mL of DI water. For NH_2CSH_2N with P.M. = 76.12 g mol^{-1}, it was prepared stock solution of Thiourea at 0.1 M in 100 mL, calculating the mass needed with **Eq.** (3.5).

$$(0.1\text{L})(1\text{mol L}^{-1})(76.12\text{g mol}^{-1}) = 0.7612\text{g} \tag{3.5}$$

$$CuSO_4 \cdot 2\,H_2O + NH_2CSH_2N \xrightarrow[H_2O/CH_3CH_2OH]{250\,^\circ C} A-\text{product} \tag{3.6}$$

The experiment steps showed below as the **Fig.** (3.1),the synthesis were prepared corresponding to the **Table** (3.2) in 250 mL beaker.

1. First, $CuSO_4 \cdot 5\,H_2O$(0.01 M) was dissolved in solvent (water/ethanol) according **Table** (3.2).
2. Then, H_2NCSNH_2 was added and stirred in the solution at 7500 rpm during 40 min and only in 11 sample was 5 mL Ethylene glycol to improve solubility.
3. Finally, the preheated glass substrates were sprayed with the solution at conditions indicated in **Table** (3.2).

Observations

The precursor solution was only for five samples can to perform with all the solution, the others samples presented precipitation in the precursor solution during the deposition.

Table 3.2: Experimental data of copper sulfide synthesis.

Sample	$CuSO_4 \cdot 5\,H_2O$ (0.01 M) mL	NH_2CSH_2N (0.1 M) mL	DI water mL	Temperature °C	Time min	Pressure psi
1	1	20	89	300 - 360	11	30
2	1	10	89	200	11	30
3	1	10	89	200 - 250	7	50
4	1	10	89	250 - 230	9	50
5	1	10	89	250	4	50
6	2	20	178	250	5	40
7	1.1	11	99	150	8	30
8	1.1	11	97.9	200	33	30
9	2.2	22	195.8	235 - 250	43	30
10	1	10	89	200 - 235	9	30
11*	2	20	173	200 - 250	30	30
12	2	20	178	200 - 250	30	30
13	1	10	79	250	15	40
14	2	20	79	250	8	40
15	1	10	79	200	8	40

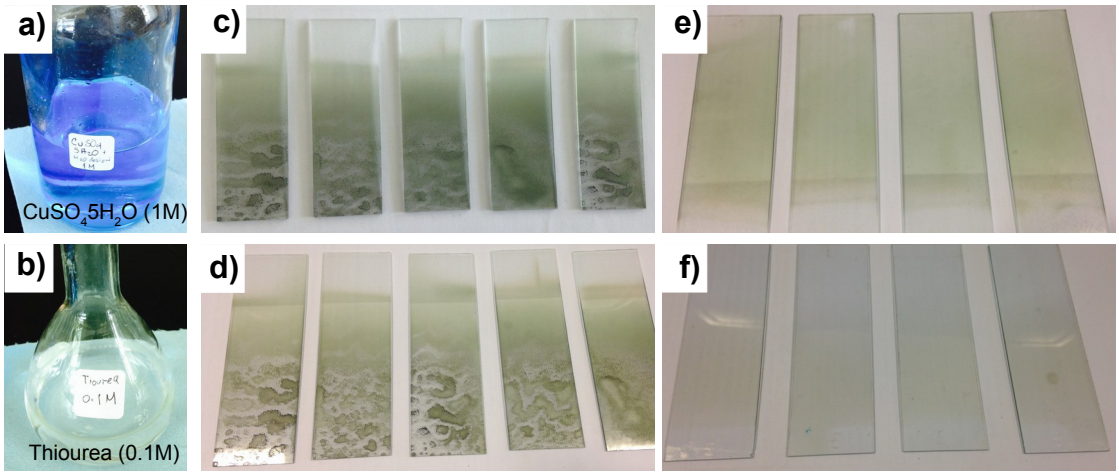

Figure 3.3: a)Stock solutions of a)$CuSO_4 \cdot 5\,H_2O$ at (1 M) concentration in 100 mL of DI water. b) Thiourea at 0.1 M in 100 mL. c) samples were prepared with — ration molar. d) samples were synthesized with — ratio molar. e) samples were prepared with – ratio molar. f) samples were prepared with — ratio molar.

3.4 Synthesis of antimony sulfide

$$Sb_2S_3 + NH_2CSH_2N \xrightarrow[H_2O/CH_3CH_2OH]{250\,^{\circ}C} B-\text{product} \tag{3.7}$$

The experiment steps as **Fig.** (3.1) were realized with the data of the **Table** (3.3).

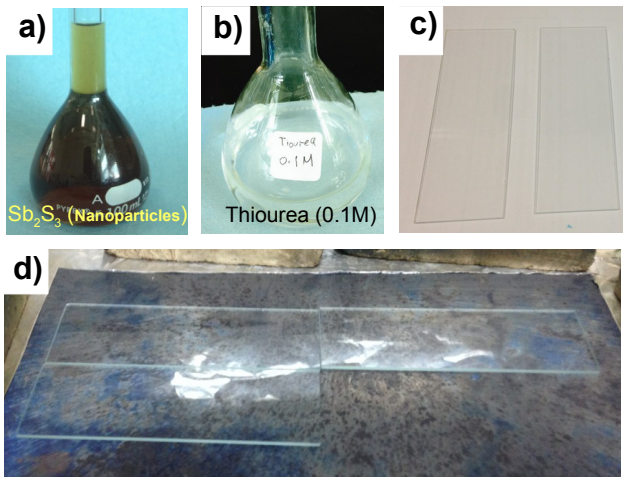

Figure 3.4: Stock solutions of a)Sb_2S_3 nanoparticles from laser ablation in 100 mL of DI water. b) Thiourea at 0.1 M in 100 mL.

1. Sb_2S_3(ac) nanoparticles were poured in a 250 mL beaker with ethanol.
2. Then, H_2NCSNH_2(ac) was aggregated in the solution.
3. After, deionized water was poured and stirred at 7500 rpm during 5 min.
4. Finally, Precursor solution was sprayed at conditions according **Table** (3.3) onto the heated substrates.

Observations

It was observed the films grew during the spray pyrolysis, but after the precursor solution was done, the substrate temperature was increased very fast even though the heater was turned off to cool the samples, the films were evaporated.

Table 3.3: Experimental data of antimony sulfide synthesis.

Sample	Sb_2S_3 mL	NH_2CSH_2N (0.1 M) mL	DI-water/Ethanol mL	Temp. °C	Time min	Pressure psi
6	10	10	30 / 50	250	12	30
7	20	20	30 / 30	250	14	30
8	30	14.5	25.5 / 30	250	16	30
9	50	14.5	25.5 / 50	270	6	30

3.5 Synthesis of $CuSbS_2$ with $(CH_3CO_2)_3Sb$ as Sb precursor

$$CuCl_2 + (CH_3COO)_3Sb + NH_2CSH_2N \xrightarrow[H_2O/CH_3CH_2OH/HCl]{250\,^{\circ}C} C-\text{product} \quad (3.8)$$

The experiment steps as **Fig.** (3.1) were realized with the data of the **Table** (3.4) and they are presented below.

1. In a 250 mL beaker with deionized water and ethanol according **Table** (3.4) for each sample, $(CH_3COO)_3Sb(aq)$ was poured.
2. Second, $CuCl_2(aq)$ was added to the solution.
3. Third, $H_2NCSNH_2(aq)$ was poured in the beaker.
4. Then,HCl was dissolved in the solution.
5. After, the solution was stirred at 7500 rpm during 20 min.
6. Finally, On the preheated substrates were sprayed the precursor solution at conditions indicated in table 3.4.

Table 3.4: Experimental data of copper antimony sulfide synthesis with $(CH_3COO)_3Sb$.

Sample #	DI water	Ethanol	$(CH_3CO_2)_3Sb$ (0.01 M)	$CuCl_2$ (0.01 M)	NH_2CSH_2N (0.1 M)	HCl	Temperature	Time
	mL	mL	mL	mL	mL	mL	°C	min
10	30	40	10	10	10	5	250-320	19
11	25	40	10	10	10	5	300-345	22
12	0	45	20	20	10	10	250-320	9
13	20	25	30	30	10	5	300-345	9

Observations

The films were formed on the substrates, but those experiments were not appropriate for the equipment, because the HCl corrodes the stainless steel nozzle. And the acid was necessary for solubility of the $(CH_3COO)_3Sb$.

3.6 Synthesis of $CuSbS_2$ using $SbCl_3$ as Sb precursor

$$CuCl_2 + SbCl_3 + NH_2CSH_2N \xrightarrow[CH_3CH_2OH]{250\,^{\circ}C} D-product \quad (3.9)$$

We obtained the $CuSbS_2$ thin films using precursor solutions were prepared with $SbCl_3$, $CuCl_2$ and H_2NCSNH_2 at different molar ratios. The experiment steps, as seen in **Fig.** (3.1), were realized with the conditions of **Table** (3.5).

1. In a 100 mL beaker, $SbCl_3$ was dissolved and stirred in ethanol (CH_3CH_2OH) at 4500 rpm during 5 min.
2. $CuCl_2$ was stirred with ethanol at 4500 rpm during 5 min in a 100 mL beaker,
3. As same, H_2NCSNH_2 was dissolved in ethanol and stirred at 4500 rpm during 5 min in a 100 mL beaker.
4. The three solutions were mixed in a 500 mL Erlenmeyer flask and then ethanol was added until 500 mL.
5. The solution was stirred at 1000 rpm at 60 °C for 5 min to dissolved it.
6. The heated substrates were sprayed with the solution at conditions indicated in **Table** (3.5).

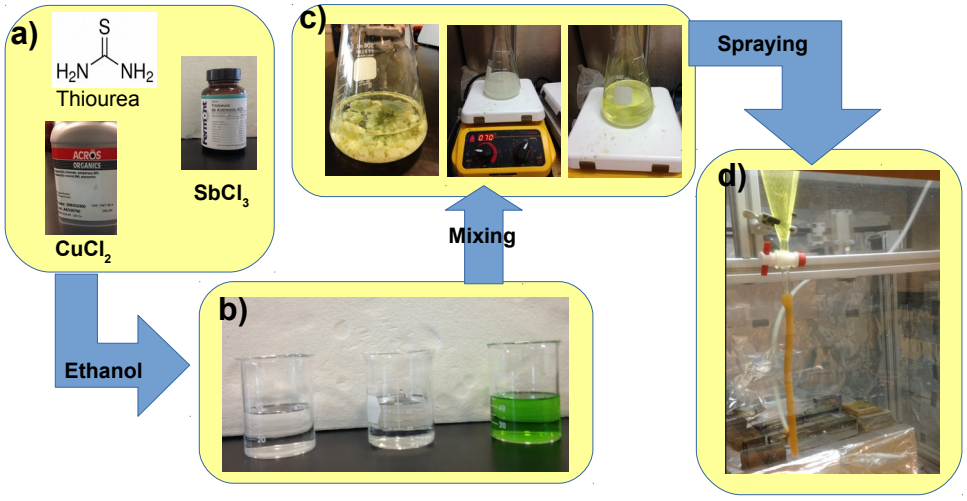

Figure 3.5: a)Reactants. b)Precursor solutions. c) Precipitated and solubility solutions. d) Sprayed solution.

Table 3.5: Experiments using $CuCl_2$,$SbCl_3$, and H_2NCSNH_2

Sample #	Molar ratio Cu : Sb : S	$CuCl_2$ (mol-L^{-1})	$SbCl_3$ (mol-L^{-1})	H_2NCSNH_2 (mol-L^{-1})	Pressure (psi)	Temperature (°C)	Volume (L)	Time (min)
14	1 : 0.96 : 05.53	0.0109	0.0104	0.0.0601	30	398	0.105	8
15	1 : 0.98 : 05.47	0.0110	0.0107	0.0.0602	30	426	0.105	31
16	1 : 0.85 : 05.01	0.0110	0.0094	0.0.0551	30	398	0.115	42
17	1 : 0.81 : 13.02	0.0104	0.0084	0.0.1359	30	382	0.250	25
18	1 : 1.02 : 05.67	0.0157	0.0160	0.0.0889	30	382	0.150	17
19	1 : 0.44 : 15.00	0.0221	0.0097	0.0.3307	30	382	0.250	61
20	1 : 0.82 : 13.20	0.0104	0.0085	0.0.1370	30	310	0.250	32
21	1 : 0.74 : 12.10	0.0114	0.0084	0.0.1382	30	310	0.250	32
22	1 : 0.84 : 12.98	0.0106	0.0089	0.0.1377	30	310	0.500	45
23	1 : 0.88 : 12.96	0.0106	0.0093	0.0.1378	30	310	0.500	46
24	1 : 0.71 : 14.30	0.0142	0.0100	0.0.2032	30	310	0.500	45
25	1 : 0.84 : 13.45	0.0107	0.0090	0.0.1440	30	310	0.250	22
26	1 : 0.97 : 12.92	0.0114	0.0109	0.0.1466	30	315	0.250	30
27	1 : 0.79 : 11.67	0.0119	0.0093	0.0.1390	30	448	0.250	30
28	1 : 0.65 : 17.31	0.0110	0.0071	0.0.1905	30	310	0.300	17
29	1 : 1.08 : 13.47	0.0100	0.0108	0.0.1348	30	310	0.250	22
30	1 : 3.86 : 47.50	0.0035	0.0136	0.0.1674	30	310	0.750	90
31	1 : 0.82 : 12.37	0.0111	0.0090	0.0.1370	30	226	0.500	22
32	1 : 0.81 : 11.64	0.0117	0.0094	0.0.1364	30	226	0.500	40
33	1 : 0.66 : 12.34	0.0124	0.0081	0.0.1527	30	226	0.250	20
34	1 : 0.46 : 08.35	0.0163	0.0074	0.0.1360	30	226	0.250	20
35	1 : 0.54 : 10.07	0.0143	0.0077	0.0.1443	30	226	0.500	40
36	1 : 0.81 : 13.02	0.0104	0.0084	0.0.1359	30	282	0.250	25

Determination of the values of the parameters for the $CuSbS_2$ synthesis

The values of the parameters were determined from the state of the art and the datasheet of the equipment. For this synthesis, we took account the following parameters:

Molar ratio: Popovici *et al.* reported a molar ratio of 1:1.48:13 with HCl for the solubility of the precursor solution and 1:1.84:13 with polymer additives as sustite of the acid [59]. Manolache *et al.* reported a molar ratio starting from

1:2.57:5.71 aggregating HCl to increase the solubility of the Antimony (III) Acetate [58]. These two reports are for spray pyrolysis deposition. We did not use HCl for this synthesis of $CuSbS_2$, but we had precipitation with the antimony acetate, so we changed for Antimony (III) chloride, and after the mixed of the precursors, we stirred and warmed at 70 °C for 30 min. Due to the sulfur loss during the pyrolytic process, the sulfur was determined as in the molar ratio of Popovici *et al.* [59]. Also we increased above 13, but the precursor solution was precipitated due to thiourea saturation.

Pressure: This parameter is constant at 30 psi due the atomization works efficiently according to the manufacturer's datasheet of the nozzle (http://www.spray.com/cat76/automatic/). The pressure can be determined with accuracy due of the graduated pneumatic valve and by the constant airflow of the laboratory. It affects the surface temperature of the substrate and the aerosol transport.

Temperature: Manolache *et al.* reported the synthesis of thin films of $CuSbS_2$ by spray pyrolysis. They obtained $CuSbS_2$ films at 240 °C with 21 psi, and they observed with X-Ray Diffraction that the crystal structure corresponds to the $CuSbS_2$ according PDF# 44-1417 [58]. Also, Thiruvenkadam *et al.* reported synthesis of $CuSbS_2$ at 300 °C with 1.40 eV. This temperature was referring to the heater temperature, we started in the range of 240 °C to 300 °C as reported in literature [58, 61].

Volume: This value was assigned since we had only one separating funnel of 0.500 L and other of 0.250 L for the containment of the precursor solution.

Deposition time: This value depends of the precursor solution volume. For 0.500 L results around 40 to 46 min and For 0.250 L results around 20 to 25 min.

4 Characterization of $CuSbS_2$ thin films

4.1 Introduction: Choosing the samples

We selected the D-17, D-22 and D-23 samples to analyze their structure, morphology, electrical, and optical properties. The conditions for the synthesis of the selected samples are given in **Table** (4.1). Visually, they present the dark gray color described by Rodríguez-Lazcano *et al.* [16] and it is visually appreciated, uniform films without porosity.

Table 4.1: Experimental conditions of D-17, D-22 and D-23 samples using $CuCl_2$,$SbCl_3$, and H_2NCSNH_2

Sample #	Molar ratio Cu : Sb : S	$CuCl_2$ (mol-L^{-1})	$SbCl_3$ (mol-L^{-1})	H_2NCSNH_2 (mol-L^{-1})	Pressure (psi)	Temperature (°C)	Volume (L)	Time (min)
17	1 : 0.81 : 13.02	0.0104	0.0084	0.0.1359	30	382	0.250	25
22	1 : 0.84 : 12.98	0.0106	0.0089	0.0.1377	30	310	0.500	45
23	1 : 0.88 : 12.96	0.0106	0.0093	0.0.1378	30	310	0.500	46

4.2 Stylus Profiler

The thin films thickness of D-17, D-22 and D-23 samples were measured using Alpha-Step D-100 Stylus Profiler. It is a equipment to record the surface profile

characteristics, specially in thin films, from the step height can be determined the thickness, where by applying a constant force in a stylus profiler, which goes up and down, amplified the signal according to the surface, at the same time, sensed by a sensor amplified and then send the data to a computer to read [1, 70].

It is an economic-rapid characterization technique that also has the advantages of no need of sample preparation and measurement through layers of different compositions [70].

The average thickness of the samples D-17, D-22 and D-23 were showed in **Table** (4.2) according to the data sheet of the equipment, the software of 2D stress analysis uses the polynomial curve fit models to calculate the heights and then it do average thickness.

In the stylus profiler for thin films, we make a scratch on the film and remove it then the profiler measured the step between the glass substrate and the film.

Table 4.2: Average thickness for samples D-17, D-22, and D-23.

Sample	Molar ratio	Volume (L)	Thickness (nm)
D-17	1.23 : 1 : 16.09	0.250	348
D-22	1.18 : 1 : 15.39	0.500	609
D-23	1.14 : 1 : 14.77	0.500	283

The D-22 and D-23 samples were prepared at similar spray rate, but they presented a 326 nm of difference in thickness between them. In spray pyrolysis deposition are several factors those affected apart from spray rate, such as substrate temperature, solution concentration and droplet radius [62, 63, 71]. These samples were formed at the same substrate temperature and similar conditions of molar ratio, at hence the change in thickness suggested by the droplet radius.

4.3 X-Ray Diffraction (XRD)

X-Ray Diffraction is used to identify the crystalline structure. We tracked the phase composition of the major, minor and traces compounds starting of the intensity peaks. The grain size (G_{size}) was obtained by the Scherrer equation.

$$G_{size} = \frac{K\lambda}{\beta cos\theta}; \tag{4.1}$$

Where K is a shape factor near of unity value, λ is the X-ray wavelength, β is the FWHM, and θ is the Bragg angle. It can be identified the preferred orientation planes.

Since thin film thickness was below 1 µm, the characterization was made by Grazing Incidence X-Ray Diffraction (GIXRD) to avoid the noise of the glass substrate. GIXRD consists of X-Ray Incidence angle (ϕ) that fixes below 1°, and the angle (2θ) between incident beam and diffracted beam was varied. The equipment for the characterization was made by a Rigaku Ultima IV diffractometer employing Cu Kα_1 radiation (λ = 1.540 59 Å).

Each sample was tested with three different grazing incidence angles (ϕ), 0.1°, 0.3° and 0.5° between scan range (2θ) of 10° to 70°.

D-17 thin film

The D-17 GIXRD pattern is shown in **Fig.** (4.1) and the planes relation in **Table** (4.3). The molar ratio was made with $1.23_{Cu} : 1_{Sb} : 16.09_{S}$. The spray pyrolysis parameters were 382 °C of substrate temperature, 0.250 L of precursor solution volume, 25 min spraying time at 30 psi of pressure.

From **Fig.** (4.1), at ϕ=0.1°, we observed two peaks, one peak at 2θ=27.96° identifying as ($\bar{4}22$)/(222) plane corresponding to Cu_2S phase according PDF# 42-1393 and other peak at 2θ=28.72° identifying as (410) plane corresponding to

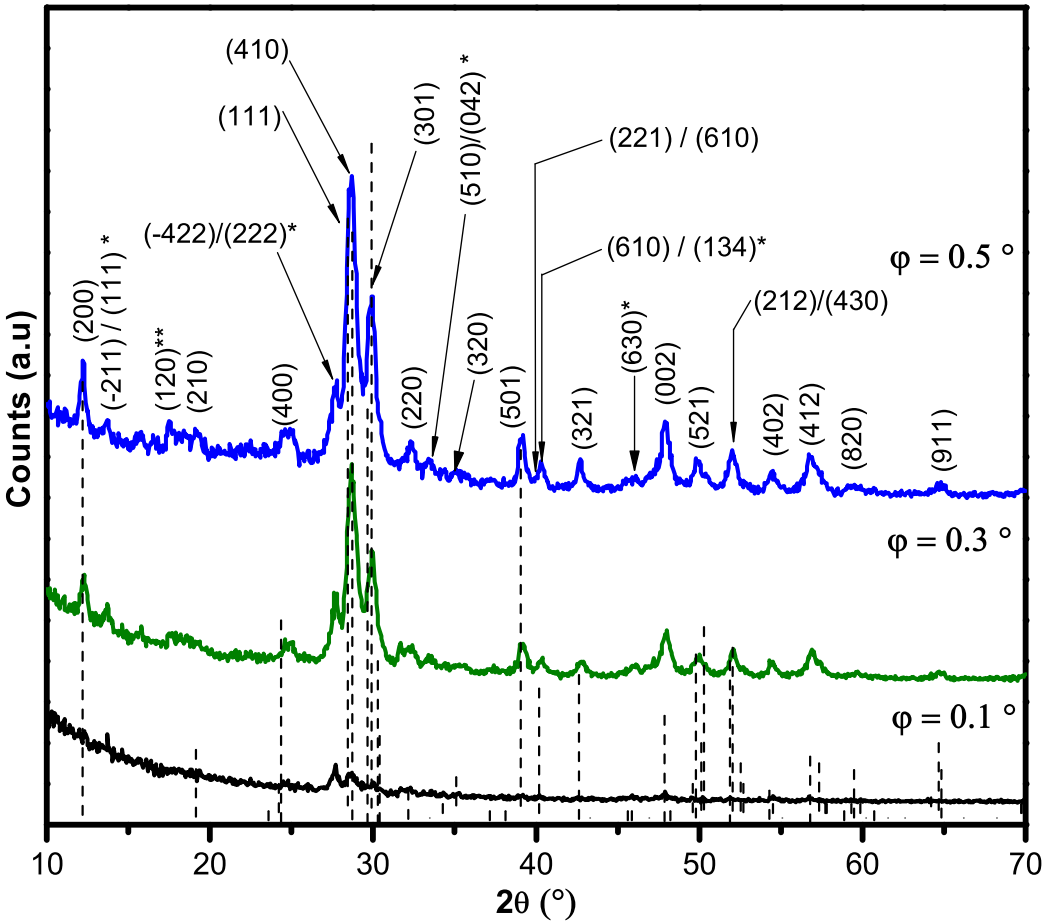

Figure 4.1: GIXRD Pattern of D-17 sample with Molar Ratio $Cu : Sb : S \rightarrow 1.23 : 1 : 16.09$ on thin film/glass substrate at ϕ(0.1°, 0.3° and 0.5°) shows the formation of orthorhombic crystal of $CuSbS_2$ phase according PDF# 44-1417. The parameter depositions were 382 °C of temperature, 0.250 L of precursor solution volume, 25 min process time at 30 psi of pressure.

$CuSbS_2$ phase according to PDF# 44-1417. With these data, we can not tracked phase composition yet.

At ϕ=0.3°, we identified the majority of the characteristic peaks of $CuSbS_2$ phase according to PDF# 44-1417. There are thirteen peaks corresponding to (200), (400), (410), (301), (220), (501), (321), (002), (521), (212)/(430), (402) and (412) planes according to the $CuSbS_2$ phase. Peaks of Cu_2S phase was also presented corresponding to ($\bar{2}$11)/(111), (510)/(042), (610)/(134), and (630) planes according to the PDF# 83-1462.

At ϕ=0.5°, there were thirteen peaks plus five more than ϕ=0.3°, corresponding of characteristics peaks of $CuSbS_2$ phase that are reported in table 4.3 and listed below (200), (210), (400), (111), (410), (301), (220), (320), (501), (221), (610), (321), (002), (521), (430), (402), (412), and (911) corresponding of the $CuSbS_2$ phase in accordance of PDF# 44-1417 (orthorhombic phase).

The form shows a preferred orientation of planes (111) and (410), since the most intensity peaks were 28.45° and 28.73° corresponding to these planes.

The Cu_2S phase was also present marked by ($\bar{2}$11)/(111), ($\bar{4}$22), (222), (042) and (510) planes (PDF# 83-1462).

(120) plane observed at 17.53° that it can be corresponding for Sb_2S_3 phase according PDF# 42-1393.

Table 4.3: Planes and phase according of 2 θ of D-17 thin film showed at ϕ=0.5°.

Planes	2 θ	Phase	Planes	2 θ	Phase	Planes	2 θ	Phase
(200)	12.20°	$CuSbS_2$	(301)	29.90°	$CuSbS_2$	(321)	42.61°	$CuSbS_2$
($\bar{2}$11)	13.87°	Cu_2S	(220)	32.17°	$CuSbS_2$	(630)	45.93°	Cu_2S
(111)	13.87°	Cu_2S	(042)	33.58°	Cu_2S	(002)	47.86°	$CuSbS_2$
(120)	17.52°	Sb_2S_3	(510)	33.58°	Cu_2S	(521)	49.78°	$CuSbS_2$
(210)	19.14°	$CuSbS_2$	(320)	35.09°	$CuSbS_2$	(212)	52.03°	$CuSbS_2$
(400)	24.35°	$CuSbS_2$	(501)	39.05°	$CuSbS_2$	(430)	52.03°	$CuSbS_2$
($\bar{4}$22)	27.96°	Cu_2S	(221)	40.16°	$CuSbS_2$	(402)	54.51°	$CuSbS_2$
(222)	27.96°	Cu_2S	(610)	40.16°	$CuSbS_2$	(412)	56.79°	$CuSbS_2$
(111)	28.44°	$CuSbS_2$	(610)	40.29°	Cu_2S	(820)	59.47°	$CuSbS_2$
(410)	28.72°	$CuSbS_2$	(134)	40.29°	Cu_2S	(911)	64.67°	$CuSbS_2$

It was calculated crystallite size around 20.11 nm using **Eq.** (4.1), at ϕ = 0.5° in peaks 28.44° and 28.72°.

D-22 Thin Film

The GIXRD pattern D-22 thin film showed in **Fig.** (4.2) and **Table** (4.4) summarized the planes and angles. The molar ratio was made with 1.18_{Cu} : 1_{Sb} : 15.39_{S}. The spray pyrolysis parameters were 310 °C of temperature, 0.500 L of precursor solution volume during 45 min by 30 psi of pressure.

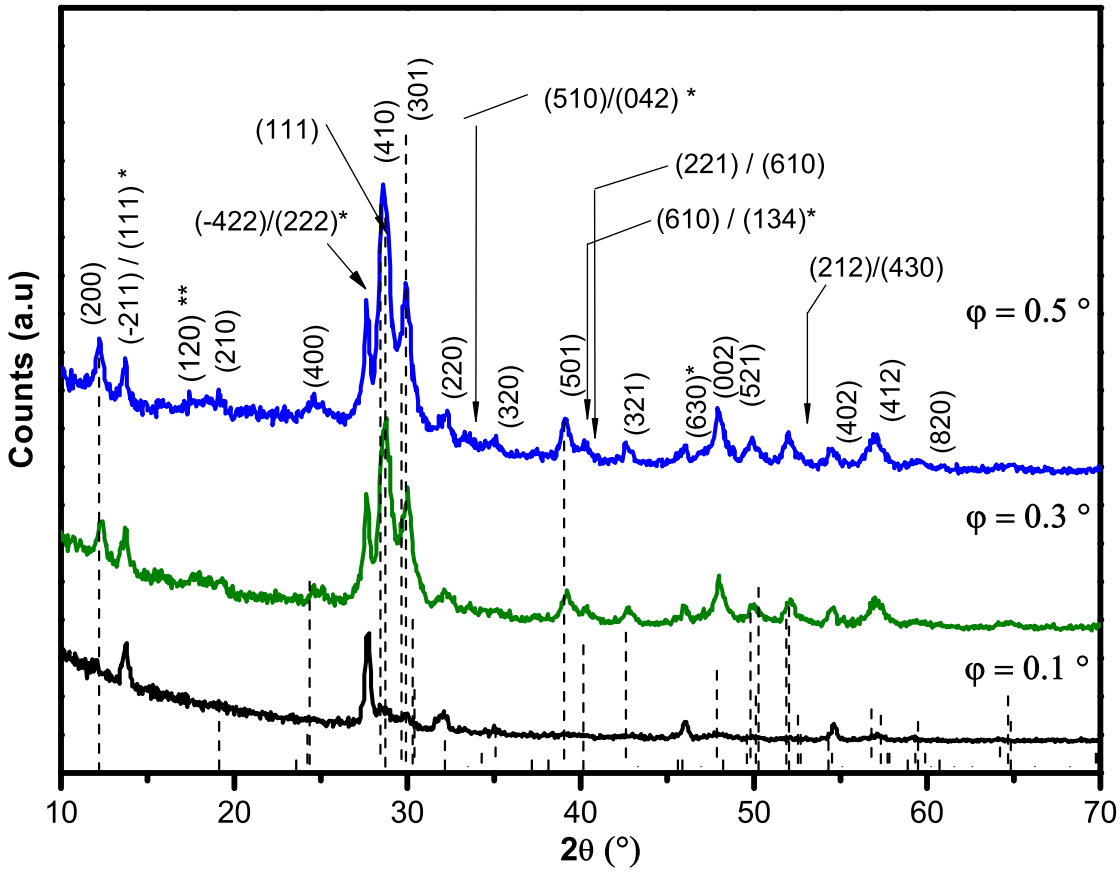

Figure 4.2: GIXRD of D-22 sample with Molar Ration Cu : Sb : $S \rightarrow 1.18 : 1 : 15.39$, at three ϕ(0.1°,0.3°, and 0.5°) shows the formation of orthorhombic $CuSbS_2$ phase.

At ϕ=0.1° few peaks presented in the pattern were $CuSbS_2$ major phase. At ϕ=0.3°, chalcostibite phase pattern was presented by most characteristic peaks of and two peaks for Cu_2S phase. At ϕ=0.5° diffractogram, it was identified the characteristic peaks corresponding of the $CuSbS_2$ phase in accordance of PDF# 44-1417 and they are shown in table 4.4.

The crystallite size was calculated of 24.41 nm using **Eq.** (4.1), in peaks 28.44° and 28.72°.

Table 4.4: Planes and 2 θ corresponding to sample D-22.

Planes	2 θ	Phase	Planes	2 θ	Phase	Planes	2 θ	Phase
(200)	12.20°	$CuSbS_2$	(301)	29.90°	$CuSbS_2$	(321)	42.61°	$CuSbS_2$
($\bar{2}$11)	13.87°	Cu_2S	(220)	32.17°	$CuSbS_2$	(630)	45.93°	Cu_2S
(111)	13.87°	Cu_2S	(042)	33.58°	Cu_2S	(002)	47.86°	$CuSbS_2$
(120)	17.52°	Sb_2S_3	(510)	33.58°	Cu_2S	(521)	49.78°	$CuSbS_2$
(210)	19.14°	$CuSbS_2$	(320)	35.09°	$CuSbS_2$	(212)	52.03°	$CuSbS_2$
(400)	24.35°	$CuSbS_2$	(501)	39.05°	$CuSbS_2$	(430)	52.03°	$CuSbS_2$
($\bar{4}$22)	27.96°	Cu_2S	(221)	40.16°	$CuSbS_2$	(402)	54.51°	$CuSbS_2$
(222)	27.96°	Cu_2S	(610)	40.16°	$CuSbS_2$	(412)	56.79°	$CuSbS_2$
(111)	28.44°	$CuSbS_2$	(610)	40.29°	Cu_2S	(820)	59.47°	$CuSbS_2$
(410)	28.72°	$CuSbS_2$	(134)	40.29°	Cu_2S			

D-23 Thin Film

In the **Fig.** (4.3), it shows the GIXRD pattern of D-23 thin film which with molar ratio of 1.14_{Cu} : 1_{Sb} : 14.79_{S} at 310 °C, of 0.500 L of precursor solution sprayed during 46 min by 30 psi.

In grazing incidence angle of 0.5°, we observed characteristics planes (200), (400), (111), (410), (301), (220), (320), (501), (221)/(610), (321), (002), (521), (212)/(430), (402), (412), and (820) as showed in **Table** (4.5) corresponding to the $CuSbS_2$ phase.

Others planes were presented by ($\bar{2}11$)/(111),($\bar{4}22$)/(222), (510)/(042), (610)/(134), and (630) corresponding to the Cu_2S phase (PDF# 83-1462). In this sample, no peak was observed corresponding to Sb_2S_3 phase.

The D-23 sample showed preferred orientation in (111) and (410) planes corresponding to $CuSbS_2$ phase, and one intensity peak in ($\bar{4}22$)/(222) corresponding to Cu_2S phase.

The calculated crystallite size was 25.59 nm at ϕ = 0.5° in peaks 28.44° and 28.72°, it was measured using **Eq.** (4.1).

Table 4.5: Planes and 2 θ corresponding to sample D-23.

Planes	2 θ	Phase	Planes	2 θ	Phase	Planes	2 θ	Phase
(200)	12.20°	$CuSbS_2$	(220)	32.17°	$CuSbS_2$	(321)	42.61°	$CuSbS_2$
($\bar{2}11$)	13.87°	Cu_2S	(042)	33.58°	Cu_2S	(630)	45.93°	Cu_2S
(111)	13.87°	Cu_2S	(510)	33.58°	Cu_2S	(002)	47.86°	$CuSbS_2$
(400)	24.35°	$CuSbS_2$	(320)	35.09°	$CuSbS_2$	(521)	49.78°	$CuSbS_2$
($\bar{4}22$)	27.96°	Cu_2S	(501)	39.05°	$CuSbS_2$	(212)	52.03°	$CuSbS_2$
(222)	27.96°	Cu_2S	(221)	40.16°	$CuSbS_2$	(430)	52.03°	$CuSbS_2$
(111)	28.44°	$CuSbS_2$	(610)	40.16°	$CuSbS_2$	(402)	54.51°	$CuSbS_2$
(410)	28.72°	$CuSbS_2$	(610)	40.29°	Cu_2S	(412)	56.79°	$CuSbS_2$
(301)	29.90°	$CuSbS_2$	(134)	40.29°	Cu_2S	(820)	59.47°	$CuSbS_2$

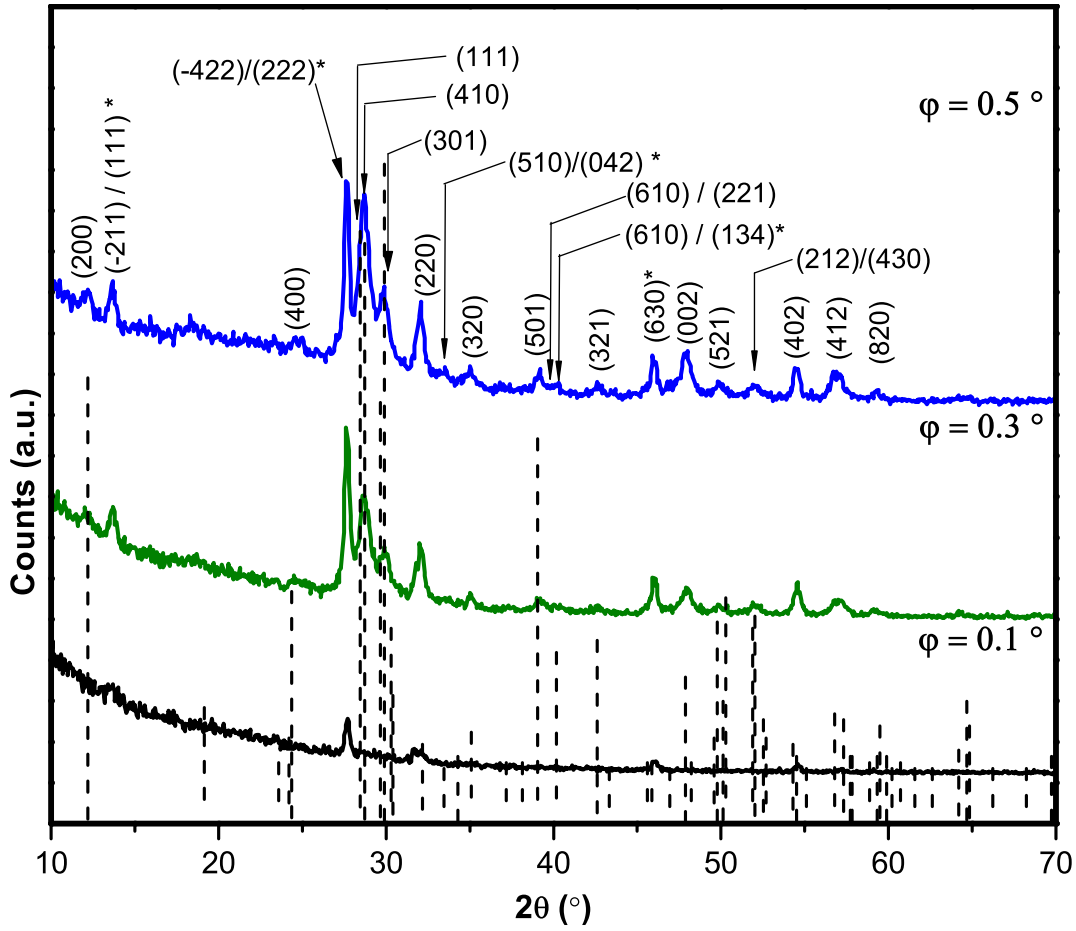

Figure 4.3: GIXRD of sample D-23 with Molar Ration $Cu : Sb : S \rightarrow 1.14 : 1 : 14.77$, with ϕ =0.1°,0.3°, and 0.5° as grazing incidence angle shows the formattion of orthorhombic crystal of $CuSbS_2$ phase.

4.4 Raman spectroscopy

It is the inelastic scattering of photons, better known as Raman scattering, where the irradiated molecules or crystals, scatter a specific vibrational spectrum being the fingerprint of the material, and it is used for structural characterization [70].

Raman spectra to the D-17, D-22 and D-23 thin films at room temperature were measured using Thermo Scientific DXR Raman Microscopy at excitation wavelength of 532 nm to identify present phases in the film as shown in **Fig.** (4.4).

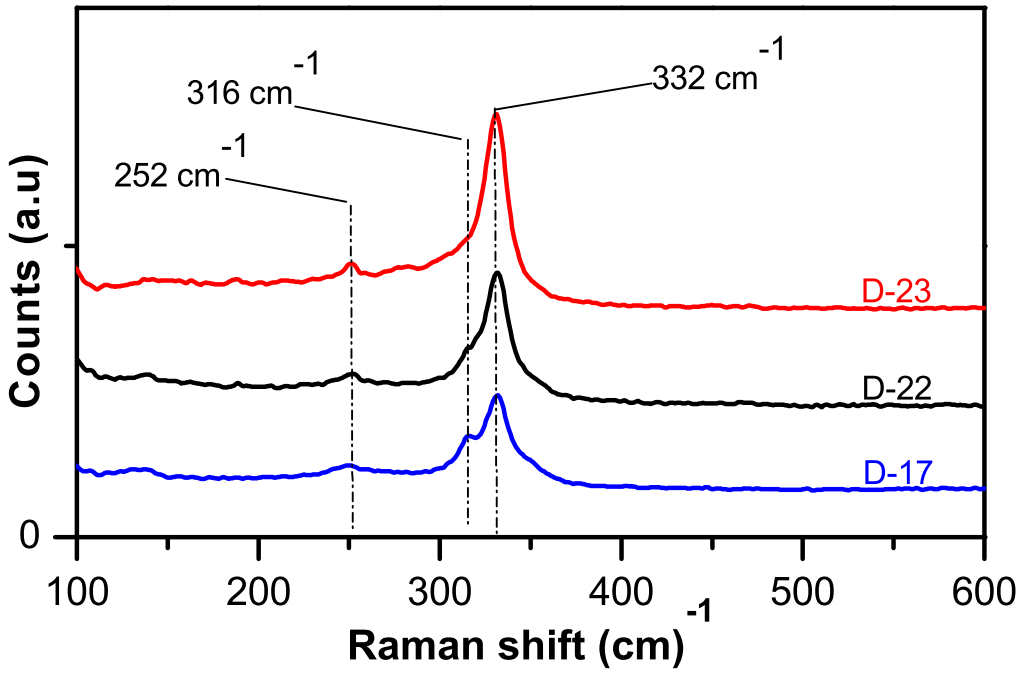

Figure 4.4: Raman spectroscopy

The peaks at 332 cm^{-1} and 252 cm^{-1}in the spectra were identified in the all the samples matched with $CuSbS_2$ phase, according to the Raman spectrum for un-oriented $CuSbS_2$ at same excitation wavelength that was published in RRUFF Project database (http://rruff.info/).

From **Fig.** (4.4), only for D-17 sample, the nearly phase pure film prepared with S\Cu precursor ratio 13.1, even the predicted low intense peak at 316 cm^{-1} was observed.

4.5 X-Ray Photoelectron spectroscopy (XPS)

Compositional analysis of thin films was done using X-ray photo-electron spectra recorded after etching by 3 keV Ar^+ ions for 60 s.

XPS is used the photoelectric effect as a fundamental, where the binding energy (E_B) of core-level electron is a result of X-ray photon energy ($h\nu$) minus the kinetic energies of the ejected photoelectrons (E_K) of the sample and the work function (Φ) of the electron spectrometer as see in **Eq.** (4.2) [72].

$$E_B = h\nu - E_K - \Phi \tag{4.2}$$

From **Fig.** (4.5) the spectras show the presence of copper at 932 eV and 952 eV in all the samples. The binding energies for antimony are identified at 529 $\pm$1 eV and 938 $\pm$1 eV in all the samples too. For the sulfur, they are identified at 161.64 $\pm$0.15 eV and 162.80 $\pm$0.15 eV.

The spectra of **Fig.** (4.5-b,4.5-c,4.5-d) showed other peaks and the corresponding elements are noted in **Fig.** (4.5-a), according National Institute of Standards and Technology (NIST) database (https://srdata.nist.gov/).

The Cl is present due of the use of synthesis for $SbCl_3$ and $CuCl_2$ as precursors. The Si, and Al are presented in the spectra because the silica (SiO_2) and the alumina (Al_2O_3) in the glass substrates defined by EN-572-1 where it gives the general chemical property of the soda lime silicate glass (http://www.glassforeurope.com/images/cont/167_32370_file.pdf), respectively. The other elements could be as contamination during the synthesis or from the precursors.

a

Binding energy (eV)	Element–Spectral Line
33	Sb 4d
51 - 53	Fe 3p
74 - 76	Al 2p 3/2
99 - 100	Si 2p
122 - 123	Cu 3s
162	S 2p
180	S 2p 3/2
190	Cl 2p
225 - 226	S 2s
496 - 497	Sn 3d
529 - 530	Sb 3d 5/2
538 - 539	Sb 3d 3/2
549 - 550	Cu LMM
569	Cu LMM
649	Mn 2p 1/2
713 - 721	Fe 2p 1/2
767 - 768	Sb 3p 3/2
932	Cu 2p 3/2
952	Cu 2p 1/2

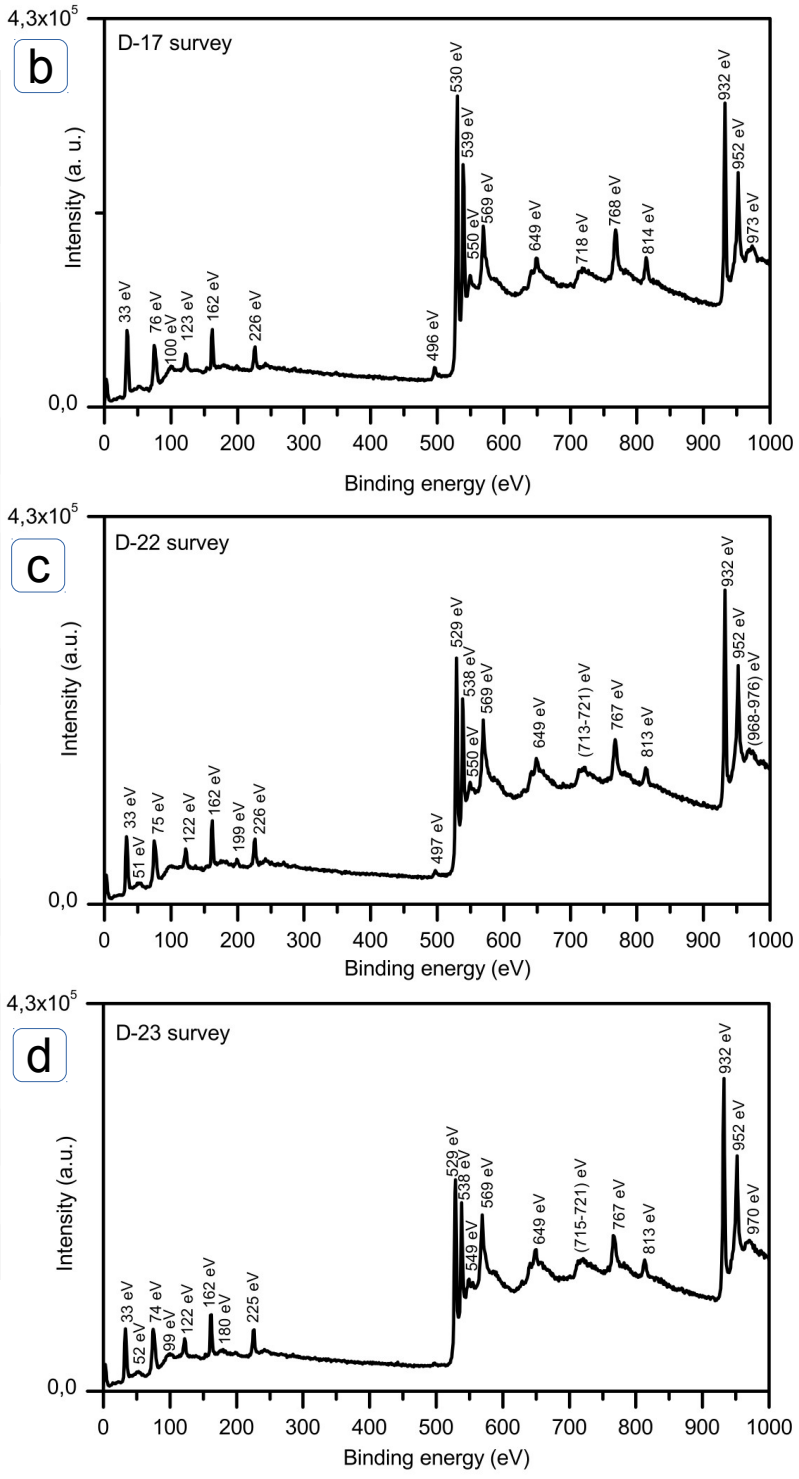

Figure 4.5: In Figure shows of: a) Binding energy and element-spectral line corresponding to D-17, D-22, D-23 sample. b) The D-17 survey on XPS. c) The D-22 survey on XPS. d) The D-23 survey on XPS.

In **Fig.** (4.6-a,4.7-a & 4.8-a) show C1s high resolution spectrum, the adventitious carbon contamination, it presents typically C−C, C−O−C and O−C=O components. As charge correction reference is used the C−C component. The carbon contamination was removed by etching with 3 keV Ar^+ ions for 60 s.

The copper, antimony and sulfur peaks were deconvoluted through Shirley type background calculation and Gaussian-Lorentzian sum function were used for peak fitting.

For Copper core level spectrum in **Fig.** (4.6-b) for D-17 showed at 932.44 eV

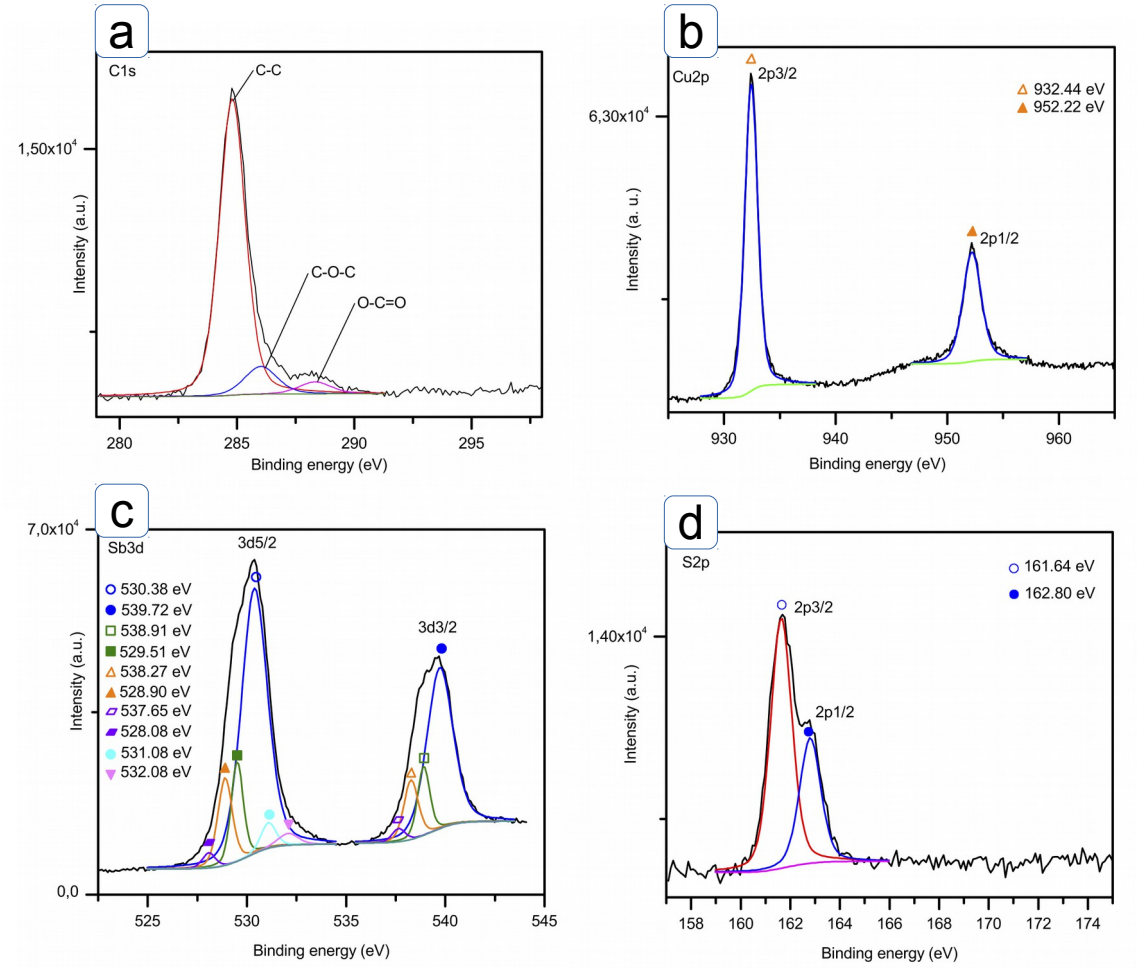

Figure 4.6: In D-17 sample obtained the high resolution spectra of: a) C1s without etched time. b) Cu2p after etching time of 60 s. c) Sb3d after etching time of 60 s. d) S2p after etching time of 60 s.

and 952.22 eV binding energies corresponding to $Cu_2p_{3/2}$ and $Cu2p_{1/2}$, respectively, only change $\pm$ 0.20 in the other samples D-22 and D-23 as showed in **Fig.** (4.7-b) and in **Fig.** (4.8-b). The spin-orbit coupling components of Cu2p peak are the$Cu2p_{3/2}$ and $Cu2p_{1/2}$ doublet present 19.8 eV distance between them. They were had an area ratio of 1 : 0.50, in the D-17 the FWHM fitted at 1.39 eV for $Cu2p_{3/2}$ and 1.93 eV for $Cu2p_{1/2}$. In D-22 the FWHM fitted at 1.32 eV for $Cu2p_{3/2}$ and 1.88 eV for $Cu2p_{1/2}$. In D-23 the FWHM fitted at 1.39 eV for $Cu2p_{3/2}$ and 1.93 eV for $Cu2p_{1/2}$.

In **Fig.** (4.6-c,4.7-c,and 4.8-c), the Sb3d shows the antimony core level spectra, which were de-convoluted into two, a doublet of $Sb3d_{5/2}$ and $Sb3d_{3/2}$. For D-17 sample showed in **Fig.** (4.6-c). There are identified four doublets with high intense peaks at (530.38 eV - 539.72 eV), (529.51 eV - 538.91 eV), (528.90 eV - 538.27 eV), and (528.08 eV - 537.65 eV) with a separation of 9.34 eV, 9.40 eV, 9.37 eV, and 9.57 eV respectively corresponding to Sb^{3+} states, as expected for $CuSbS_2$. The two weak peaks at 531.08 eV and 532.08 eV were assigned to O1s peak.

For D-22 sample analysis is shown in **Fig.** (4.7-c). There were three doublets identified with high intense peaks at (529.17 eV - 538.50 eV), (530.61 eV - 539.90 eV), and (528.18 eV - 537.68 eV) with a separation of 9.33 eV, 9.29 eV, and 9.50 eV, respectively corresponding to Sb^{3+} states, as expected for $CuSbS_2$. For D-23 sample showed in **Fig.** (4.8-c). Three doublets with high intense peaks at (528.94 eV - 538.25 eV), (530.49 eV - 539.66 eV), and (528.16 eV - 537.45 eV) with a separation of 9.31 eV, 9.17 eV, and 9.29 eV were spotted out, respectively corresponding to Sb^{3+} states, as expected for $CuSbS_2$. The weak peak at nearly 531 eV corresponds to O1s peak.

For sulfur core level spectrum shows doublet with a separation of 1.2 eV, the reported B.E. values for S^{2-} in $CuSbS_2$ as see in **Fig.** (4.6-d) at 161.64 eV and 162.80 eV binding energies corresponding to $S2p_{3/2}$ and $S2p_{1/2}$, respectively. In Fig. 4.7-d for D-17 showed at 161.58 eV and 162.77 eV and in **Fig.** 4.8-d for D-

17 showed at 161.40 eV and 162.56 eV, so the change between the samples are only change $\pm$ 0.30 at $S2p_{3/2}$ and $\pm$ 0.25 at $S2p_{1/2}$, these values at maximum and minimum in the samples D-17, D-22 and D-23. In Cu-Sb-S system, there can be other phases such as Cu_3SbS_3 and Cu_3SbS_4. However, combining our results of the B.E. values of Cu2p, Sb3p and S2p core levels and of the phases detected in our XRD results, we assigned the values for the formation of $CuSbS_2$.

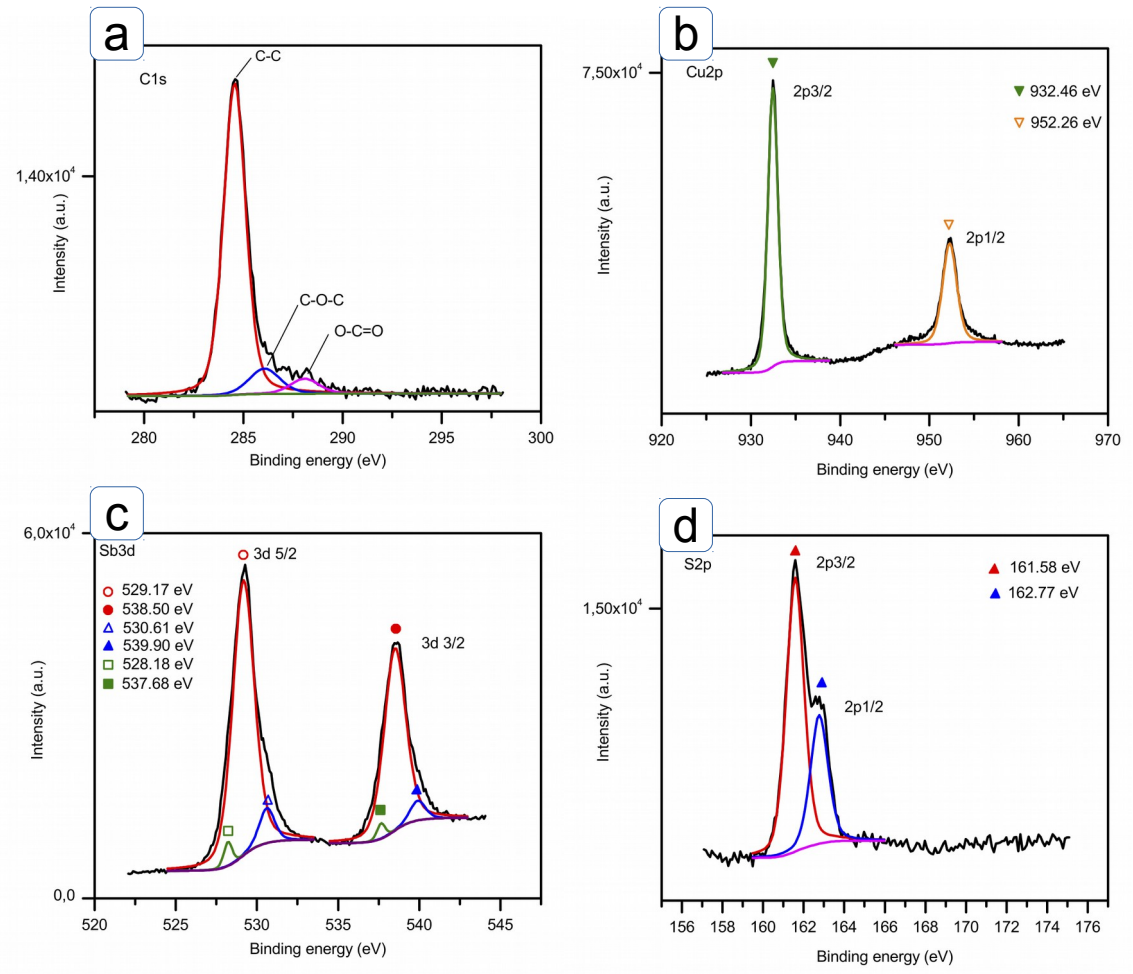

Figure 4.7: In D-22 sample obtained the high resolution spectra of: a) C1s without etched time. b) Cu2p after etching time of 60 s. c) Sb3d after etching time of 60 s. d) S2p after etching time of 60 s.

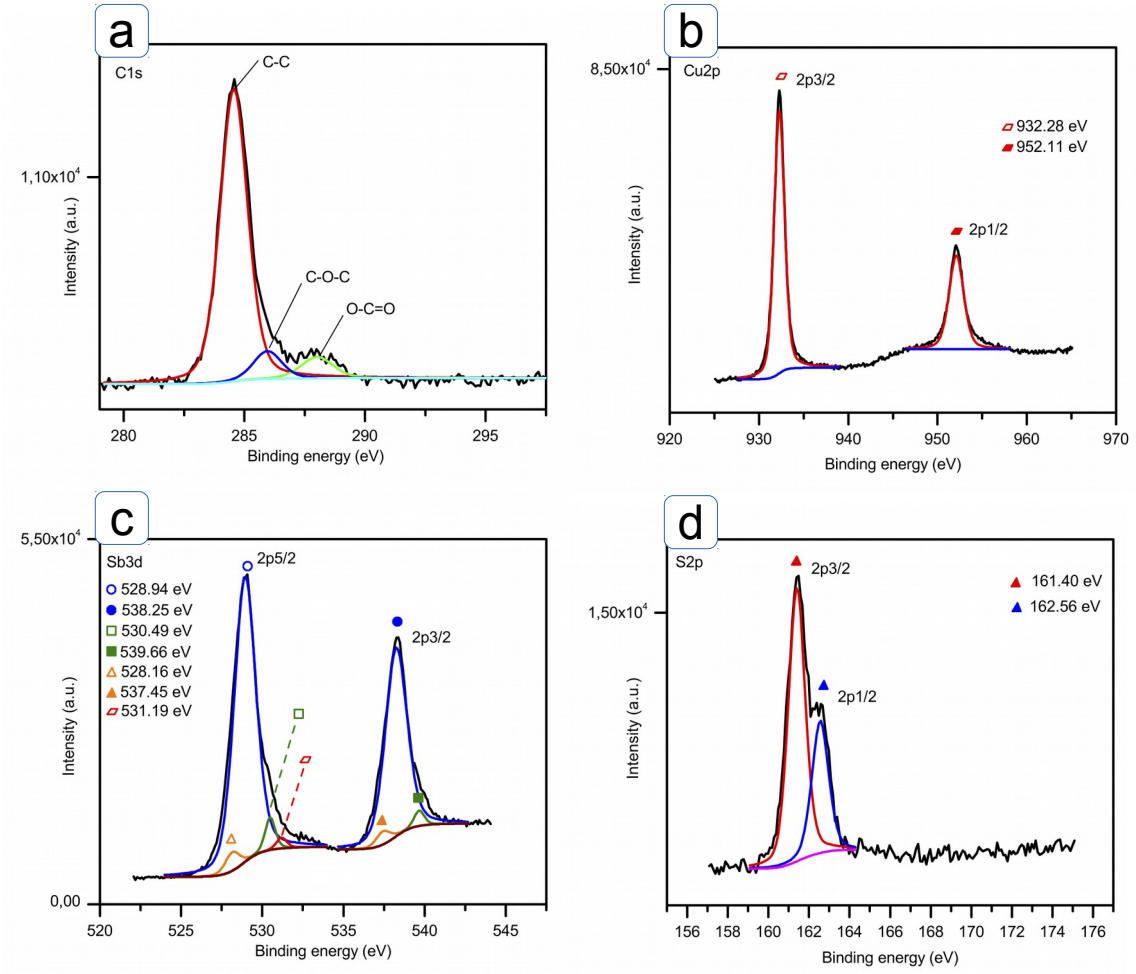

Figure 4.8: In D-23 sample obtained the high resolution spectra of: a) C1s without etched time. b) Cu2p after etching time of 60 s. c) Sb3d after etching time of 60 s. d) S2p after etching time of 60 s.

4.6 Atomic Force Microscopy (AFM)

This technique measures the surface morphology by scanning over sample surface with a sharp probe, acquiring the height data of the surface [73]. The advantages of AFM are the amplification of the axes in three dimension, no treatment needed for samples, measurement in ambient atmosphere and works for conductive or insulating samples [73].

All the samples were measured in semi-contact mode in Solver Pro, NT-MDT atomic force microscope. Morphological features of the nearly pure phase $CuSbS_2$ thin film is illustrated by 1.5 µm x 1.5 µm atomic force micrographs for the three samples (D-17,D-22 & D-23).

The direct morphology image displayed in Fig. (4.9-a) shows spherical and compact grains in a range of 20 nm to 100 nm diameter. In Fig. (4.9-b), the sample presents different grain heights in the z axis but the most of them below 150 nm.

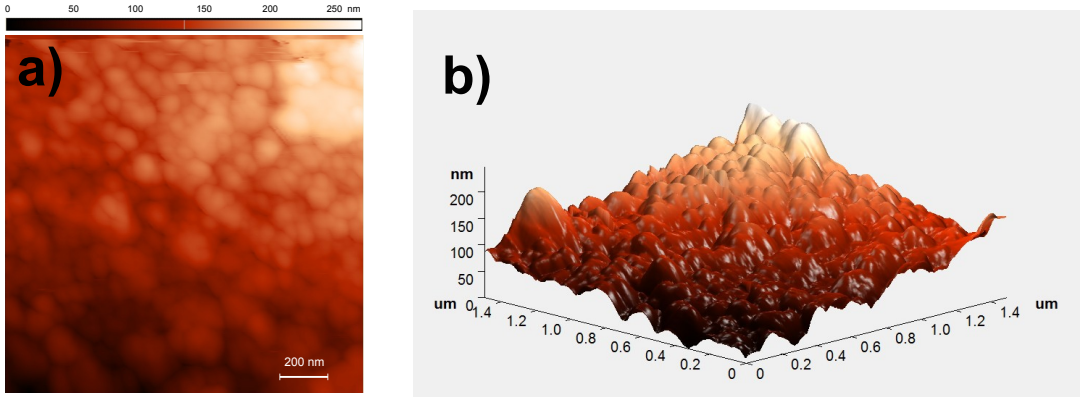

Figure 4.9: (a)AFM of $CuSbS_2$(D-17) with 1.5 micrometers. (b) AFM of $CuSbS_2$(D-17) in 3D of 1.5 micrometers.

The micrograph of D-22 sample have a very compact morphology with bigger grains than D-17 sample as can be seen in **Fig.** (4.10-a). Unlike D-17 sample, the 3D data of D-22 sample shows the majority of grains above 150 nm and grain diameters of 100 nm to 200 nm approximately.

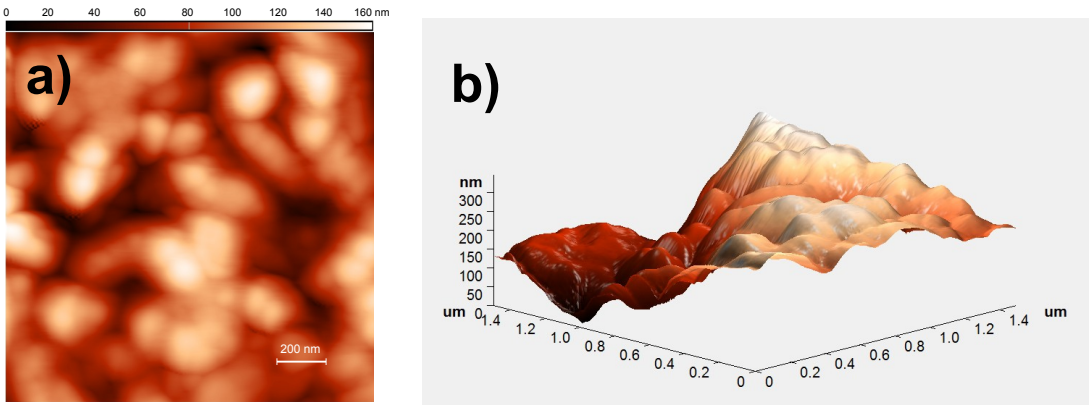

Figure 4.10: (a)AFM of $CuSbS_2$(D-22) with 1.5 micrometers. (b) AFM of $CuSbS_2$(D-22) in 3D of 1.5 micrometers.

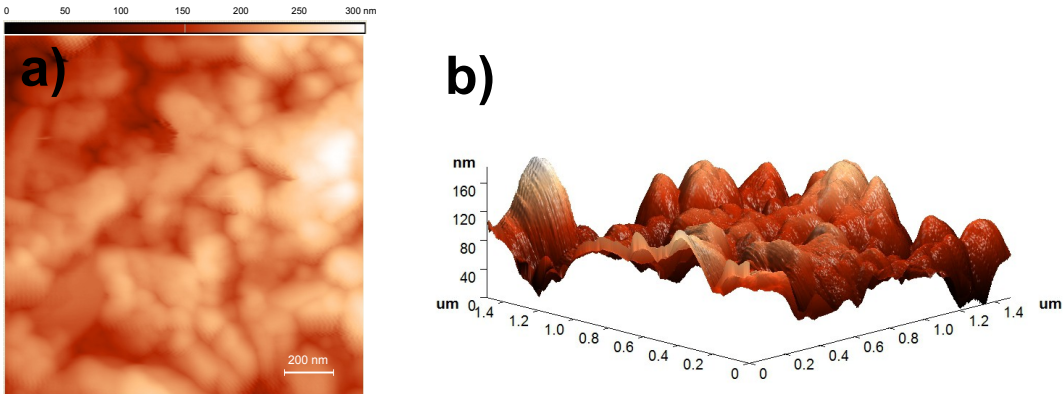

Figure 4.11: (a)AFM of $CuSbS_2$(D-23) with 1.5 micrometers. (b) AFM of $CuSbS_2$(D-23) in 3D of 1.5 micrometers.

The morphology of D-23 sample presents compact spherical grains with diameters between 100 nm to 200 nm as can be seen in **Fig.** (4.11-a). The z-axis of 3D of **Fig.** (4.11-b) gives heights from 40 nm to 180 nm. It can be concluded, that the surfaces of the thin films are not uniform and in consequence, their thickness are not uniform.

4.7 UV-visible Spectroscopy (UV-Vis)

The optical transmittance spectra and the optical reflectance spectra of the thin films were measured using an UV-Vis-NIR spectrometer of the trademark Stellarnet Inc. of the Model DXR-UVN-512.

knowing the thickness, the absorption coefficient at each wavelength was calculated. The optical band gap value of the thin film was determined using the relation **Eq.** (2.2).

In D-17, the transmittance and reflectance spectras recorded in the wavelength range of 300 nm to 1100 nm, they are shown **Fig.** (4.12). In transmittance we observed that at 300 nm started with 10 % and it increased until 50 % at 1100 nm. For Reflectance, it started at 5 % for 300 nm and it started gradually increased until 850 nm at 33 %, where the slope of the curve changed drastically.

The **Fig.** (4.12-c) illustrate in (a), the plot of α vs. wavelength, and in (b), the plot of $(\alpha h\nu)^2$ vs. $h\nu$ (Tauc plot) for the nearly phase pure sample giving good linear fit for $n = 2$. This implies that the fundamental optical absorption in the $CuSbS_2$ thin films is dominated by direct allowed transition. From the curve, the value of band gap was estimated 1.59 eV by extrapolating the linear region of the respective plot to $\alpha = 0$, as shown in the figure. This value agrees with reported value of 1.5 eV on optical properties of $CuSbS_2$, both theoretical [41, 45] and experimental values [39, 43, 46].

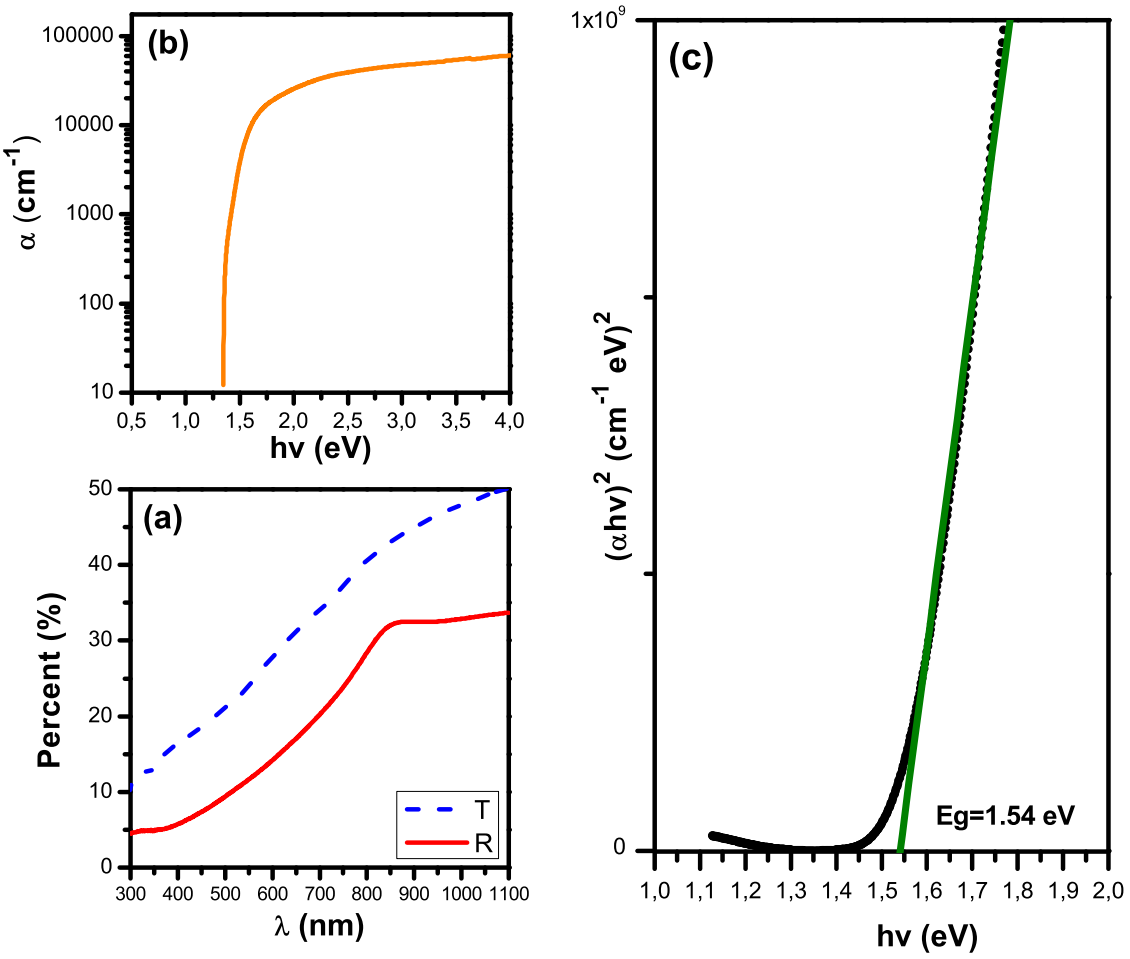

Figure 4.12: a) Transmittance and Reflectance spectrums measured. b) Absorption coefficient spectrum calculated. c) Bandgap for D-17 thin film in UV-Visible.

In the D-22 optical spectrum measurements were realized using the absorbance spectrum recorded for the same wavelength range, as shown **Fig.** (4.13), we did the measurement of the transmittance and the reflectance for the D-22 thin film. In transmittance we observed that in the range of 300 nm to 600 nm, the value was near of 0 % and it started to increase after 600 nm until 15 % at 1100 nm. Reflectance showed same behavior, it started at less than 5 % for 300 nm and it started gradually increased until a maximum of 11 % at 1100 nm.

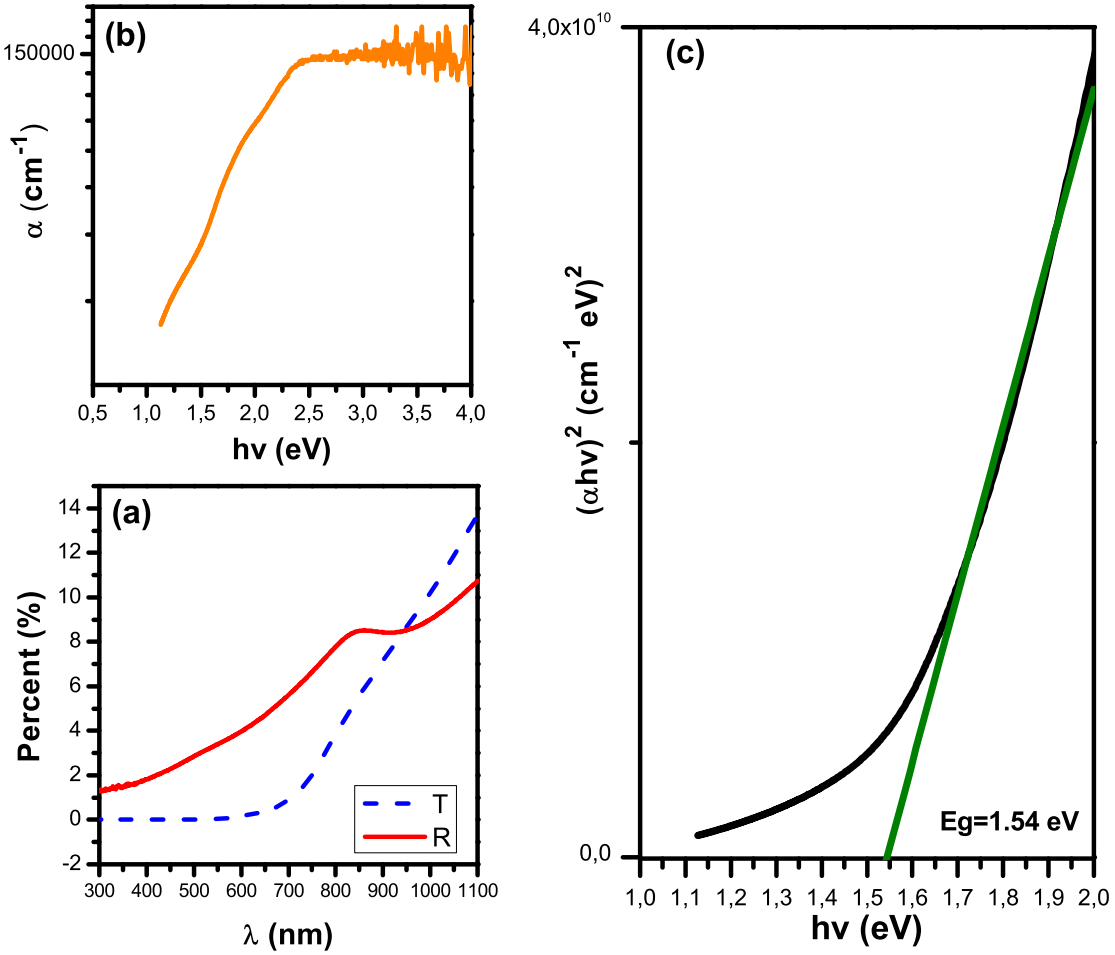

Figure 4.13: a) Transmittance and Reflectance spectrums measured. b) Absorption coefficient spectrum calculated. c) Bandgap for D-22 thin film in UV-Visible.

The **Fig.** (4.13-c) illustrate in (a), the plot of α vs. wavelength, and in (b), the plot of $(\alpha h\nu)^2$ vs. $h\nu$ (Tauc plot) for the nearly phase pure sample giving

good linear fit for $n = 2$. This implies that the fundamental optical absorption in the $CuSbS_2$ thin films is dominated by direct allowed transition. From the curve, the value of band gap was estimated 1.54 eV by extrapolating the linear region of the respective plot to $\alpha = 0$, as shown in the figure. This value agrees with reported value of 1.5 eV on optical properties of $CuSbS_2$, both theoretical [41, 45] and experimental values [39, 43, 46].

In the D-23 optical spectrum measurements were realized using the absorbance spectrum recorded for the wavelength range of 300 nm to 1100 nm, as shown **Fig.** (4.14), we did the measurement of the transmittance and the reflectance for the D-23 thin film. In transmittance we observed that in the range of 300 nm to 700 nm, the value was increased between the range of 9 % to 15 %, then the slope changed and it started to increase more so between the range of 700 nm to 1100 nm the transmittance started at 15 % and end in 30 %. For Reflectance, it showed inverse behavior, it started with a bigger slope from 3 % to 15 % and then decreased the slope at 800 nm to 1100 nm near of 15 % of reflectance.

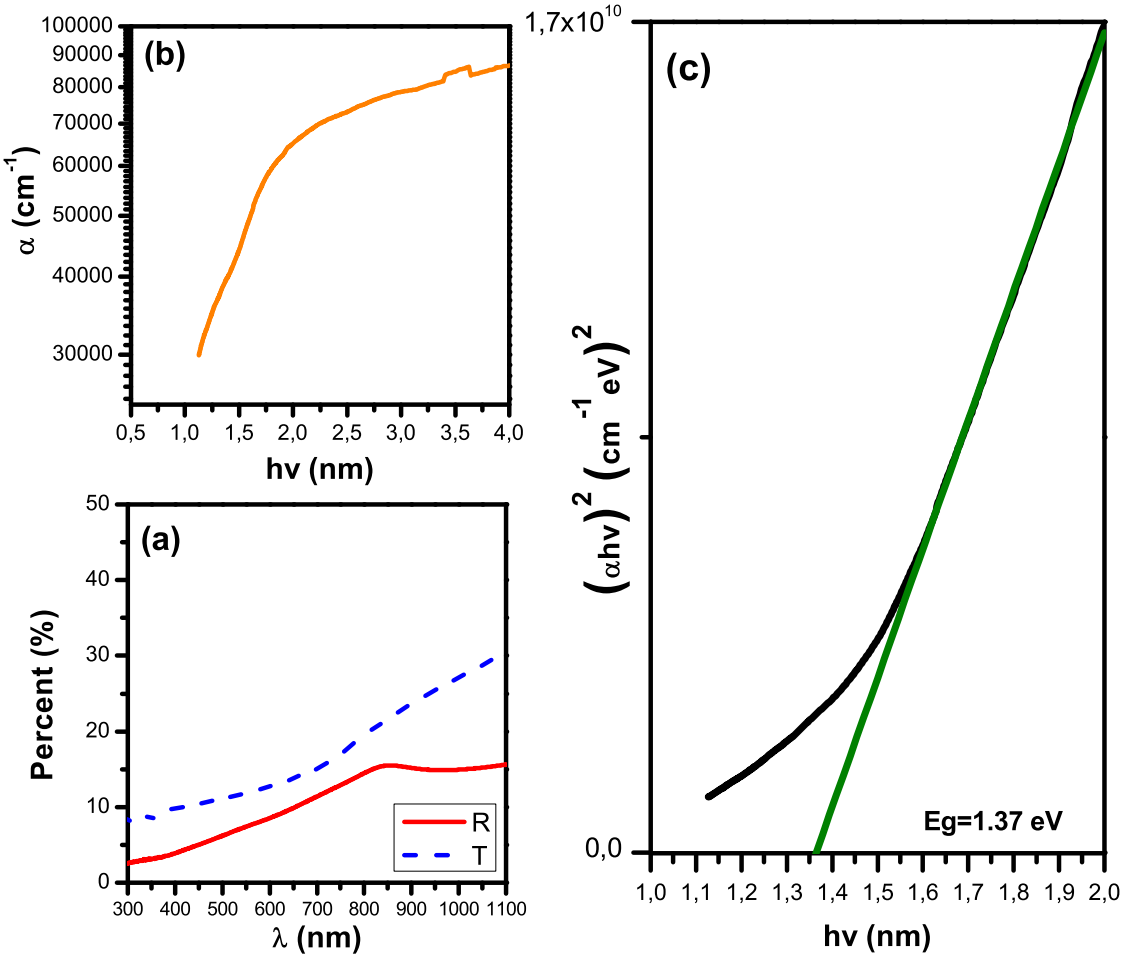

Figure 4.14: a) Transmittance and Reflectance spectrums measured. b) Absorption coefficient spectrum calculated. c) Bandgap for D-23 thin film in UV-Visible.

The **Fig.** (4.14-c) illustrate in (a), the plot of α vs. wavelength, and in (b), the plot of $(\alpha h\nu)^2$ vs. $h\nu$ (Tauc plot) for the nearly phase pure sample giving good linear fit for $n = 2$. This implies that the fundamental optical absorption in the $CuSbS_2$ thin films is dominated by direct allowed transition. From the curve, the value of band gap was estimated 1.39 eV by extrapolating the linear region of the respective plot to $\alpha = 0$, as shown in the figure. This value agrees with reported value of 1.5 eV on optical properties of $CuSbS_2$, both theoretical [41, 45] and experimental values [39, 43, 46].

4.8 Photoresponse

The photoresponse characterization is important to visualize if the material was response time and sensitivity of photoresponse materials [74]. The response time is the time required to increase For the Direct Current (dc) conductivity measurements the contacts used were two planar electrodes of 3 mm in length and 3 mm in separation using conductive silver paint, (SPI Supplies).

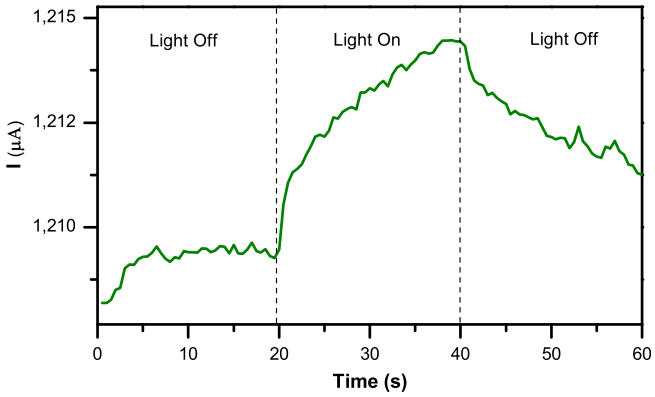

Figure 4.15: D-17 sample on Photoresponse curve

The **Fig.** (4.15,4.16,4.17) show the photoresponse of D-17, D-22 and D-23 thin films at room temperature by applying a dc bias of 5 V.

First, current was measured in darkness for 20 s, then under illuminated for 20 s, and finally in darkness for another 20 s. The three samples showed photoresponse.

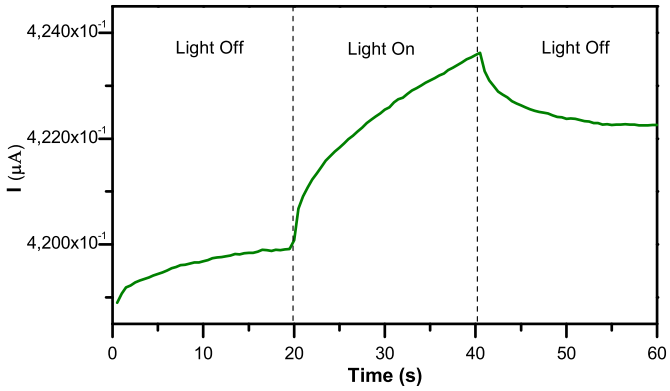

Figure 4.16: D-22 sample on Photoresponse curve

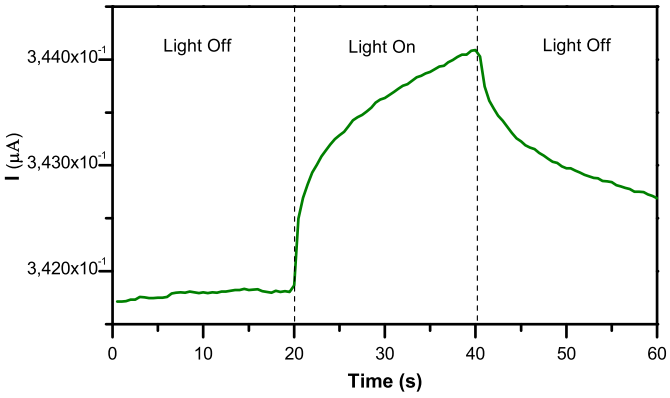

Figure 4.17: D-23 sample on Photoresponse curve

4.9 Hall Effect

The electrical properties of the thin films were measured using the Hall effect. The Hall effect is physical phenomenon occurred in metals and semiconductors when an electric current (Jx) was flowing in x direction across a rectangular bar and it applies an perpendicular magnetic field (Bz) in z direction. It exists a deflection of the charge carriers due to the Lorentz force. The deflected charge carriers accumulate on both of the y directions of the bar, generating a transverse electric field (Ey) that cancels the Lorentz force and exerts a voltage in the same direction. This voltage is called the Hall voltage and the electric field is named the Hall electric field [8, 75, 76].

The growth of D-17, D-22 and D-23 thin films are nonuniform as noted by AFM, we used the Van Der Pauw technique. It is convenient for these irregular morphology. In the samples are square and we painted four contacts (1,2,3,4) in the corners. We applied an electric current in contacts 3 to 4 and everted a magnetic field at perpendicular way. The Hall voltage was measured in contacts 1 to 2, these are perpendicular to the electric current and the magnetic field [77]. In the Van der Pauw technique can be estimated the Hall coefficient(R_H) with **Eq.** (4.3), where d is the film thickness, B is the magnetic field, and I_{34} is the electric current flowing from contact 3 to contact 4.

$$R_H = \frac{[V_{12}(B) - V_{12}(0)]d}{I_{34}B} = \frac{[V_{12}(B) - V_{12}(-B)]d}{2I_{34}B} \tag{4.3}$$

To calculate the carrier concentration (n) is used **Eq.**(4.4), where e is the charge of the electron.

$$n = \frac{1}{R_H e} \tag{4.4}$$

Yang *et al.* reported a conductivity of 20.83 $(\Omega cm)^{-1}$, a hole mobility of 49 $(\frac{cm^2}{Vs})$ and a carrier concentration of 2.66 $\times$ 10^{18} (cm^{-3}). They commented that their high hole mobility is due hole concentration [39].

Garza *et al.* reported for $CuSbS_2$ films with p-type conductivity. Their measurements showed a conductivity of 60 $(\Omega cm)^{-1}$, a mobility of 0.01 $(\frac{cm^2}{Vs})$ and a carrier

concentration of 3.9×10^{18} (cm^{-3}) in 30 nm of thickness. In thin film of 40 nm reported a conductivity of 9 $(\Omega cm)^{-1}$, a mobility of 0.001 $(\frac{cm^2}{Vs})$ and a carrier concentration of 6.1×10^{19} (cm^{-3}). And 50 nm thin film, they reported a conductivity of 0.5 $(\Omega cm)^{-1}$, a mobility of 0.1 $(\frac{cm^2}{Vs})$ and a carrier concentration of 1.4×10^{20} (cm^{-3}) [31].

The $CuSbS_2$ thin films were measured using an Ecopia HMS-3000 Hall measurement system at room temperature applying a fixed magnetic field of 0.55 T on samples with four corners painted with silver as showed in **Fig.** (4.18). Were calculated the carrier concentration (cm^{-3}), mobility ($cm^2/V\,s$) and conductivity ($\Omega^{-1}\,cm^{-1}$).

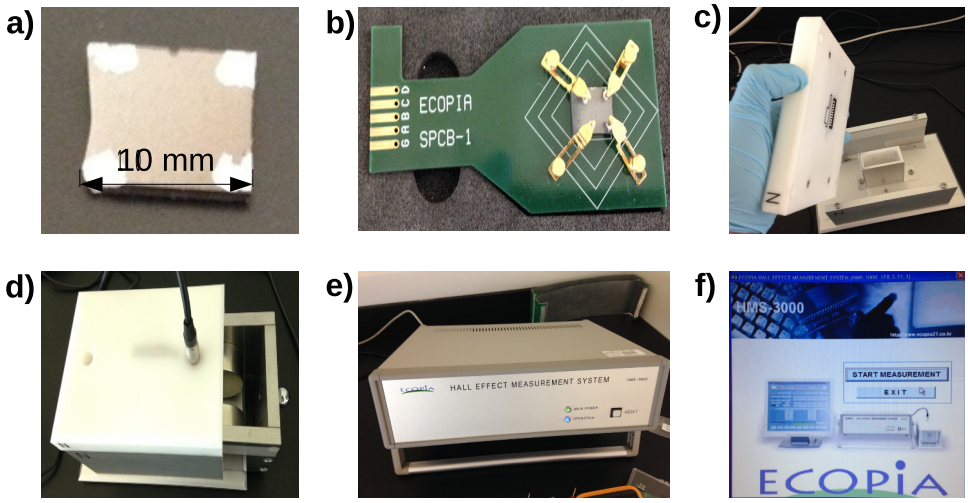

Figure 4.18: a) Sample of 1 cm x 1 cm. b) Sample adapter of Ecopia SPCB. c) Dispositive where board is inserted. d) Then it is connected to the hall effect system. e) Hall effect measurement system. f) The HMS-300 software.

Table (4.6) shows the results of D-17, D-22 and D-23 samples. All of which do have positive Hall coefficients, proving that they are p-type films. Only the D-22 sample shows a higher value than reported by Garza *et al.*, the others show similar results [31]. The conductivity is less than the reported by Yang *et al.*.

Table 4.6: Carrier concentration, mobility, conductivity and Hall Coefficient are shown of the $CuSbS_2$ thin films at 10 (μA). The Hall Coefficients are positive in all the samples corresponding to a p-type conduction.

Sample	Carrier-concentration (cm^{-3})	Mobility ($\frac{cm^2}{Vs}$)	Conductivity $((\Omega cm)^{-1})$	Hall Coefficient (cm^3/C)
D-17	1.446×10^{21}	3.324×10^{-2}	7.739	4.318×10^{-3}
D-22	1.793×10^{18}	2.630	0.755	3.482
D-23	6.389×10^{20}	1.362×10^{-2}	1.394	9.770×10^{3}

5 Conclusions

5.1 Conclusions

Material

The $CuSbS_2$ thin films were prepared on glass substrates at 300 °C to 382 °C by spray pyrolysis using the precursor solutions containing $SbCl_3$, $CuCl_2$, $CS(NH_2)_2$.

- The samples formed from precursor solutions Cu:Sb:S molar ratio: [1.23:1:9.16] [1.18:1:15.39] and [1.14:14.77:1] were analyzed.

Characterizations

These results show that thin films $CuSbS_2$ different optoelectronic properties can be obtained using the spray pyrolysis technique by varying the precursor compositions [78].

- The thickness was measured with a Stylus Profiler. The D-17 sample was prepared with 0.250 L of precursor solution and it was measured 348 nm. The D-22 sample was prepared with twice of the volume of D-17 sample, and proportional it was measured 609 nm. Not so the D-23 sample, which has a volume of 0.500 L and the thickness resulted in 283 nm, perhaps because the surface temperature of the substrate can not be accurately controlled, could have affected the growth of the film.

- The XRD showed chalcostibite crystal structure $CuSbS_2$ and Cu_2S as minor phase.
- Raman spectral analysis confirmed the compound $CuSbS_2$ phase.
- The XPS indicated the presence of copper, antimony and sulfur.
- The atomic force micrographs of the three samples (D-17/D-22/D.23) showed a spherical and compact grains. There were grains in the range of 20 nm to 100 nm in D-17 sample. Bigger grains around 200 nm in D-22 sample. For the D-23 sample, its grains were in the range of 100 nm to 200 nm in size. The AFM showed that the morphologies of the samples were composed of compact grains.
- In the UV-Vis characterization, the D-17 thin film showed an E_g = 1.54 eV. The bandgap for the D-22 was 1.54 eV and for the D-23 was 1.37 eV. These values are agree in according of the reported literature [39, 43, 46].
- The Photoresponse showed that all the thin films were photoconductive.
- Hall effect measurements showed the p-type conductivity for these samples with good carrier concentration. The D-17 presented a 7.739 $(\Omega cm)^{-1}$ conductivity. The D-22 presented a 0.755 $(\Omega cm)^{-1}$ conductivity. The D-23 presented a 1.394 $(\Omega cm)^{-1}$ conductivity.

Spray Pyrolysis

The spray pyrolysis machine was tested with a wide values for the suitable parameters for solution precursor deposition to obtain uniform thin films of $CuSbS_2$ at substrate temperature of 310 °C to 382 °C .

- The pressure for the air supply to the transportation system of the precursor solution to the substrate atomizer was set at 30 Psi, as best nucleation on the substrate surface for forming thin film was shown. At higher pressure, the

solution was spread out leaving the substrate film formation. A lower pressure, the solution accumulated on the film and not let be the right pyrolysis process for the homogeneous formation on the substrate.

5.2 Future work

- Standardize the deposition of the $CuSbS_2$ thin films by to replace full cone to flat even nozzles, to replace the separating funnel by a suitable container and to fit a ceramic container for the glass substrates.
- To realize thin film solar cell of $CuSbS_2$ by spray pyrolysis deposition.

6 Publication

Jose Agustin Ramos Aquino, Dorian Leonardo Rodriguez Vela, Sadasivan Shaji, David Avellaneda Avellaneda, and Bindu Krishnan. Spray pyrolysed thin films of copper antimony sulfide as photovoltaic absorber. Physica Status Solidi (C), 13(1):24–29, 2016.

Bibliography

[1] Jose Agustin Ramos Aquino, Dorian Leonardo Rodriguez Vela, Sadasivan Shaji, David Avellaneda Avellaneda, and Bindu Krishnan. Spray pyrolysed thin films of copper antimony sulfide as photovoltaic absorber. *Physica Status Solidi (C)*, 13(1):24–29, 2016.

[2] Vasilis Fthenakis. Sustainability of photovoltaics: The case for thin-film solar cells. *Renewable and Sustainable Energy Reviews*, 13(9):2746–2750, 2009.

[3] K L Chopra, P D Paulson, and V Dutta. Thin-film solar cells: an overview. *Progress in Photovoltaics: Research and Applications*, 12(23):69–92, 2004.

[4] Martin A. Green. Thin-film solar cells: review of materials, technologies and commercial status. *J Mater Sci: Mater Electron*, 18:15–19, 2007.

[5] Chetan Singh Solanki. *Solar photovoltaics. Fundamentals, technologies and applications*. PHI Learning private limited, second edition, 2013.

[6] A Goswami. *Thin Film Fundamentals*. New Age International Pub, 1996.

[7] P. Arunkumar, Sushil Kumar Kuanr, and K. Suresh Babu. Thin Film Structures in Energy Applications. chapter Thin Film:. Springer International Publishing.

[8] M.A. Omar. *Elementary Solid State Physics: Principles and Applications*. Addison-Wesley Publishing Company, 1993.

[9] Siegfried Eigler and Andreas Hirsch. Chemistry with graphene and graphene oxide - Challenges for synthetic chemists. *Angewandte Chemie - International Edition*, 53(30):7720–7738, 2014.

[10] L E Smart and E A Moore. *Solid State Chemistry: An Introduction, Third Edition*. E-Books von NetLibrary. Taylor & Francis, 2005.

[11] Antonio Luque and Steven Hegedus, editors. *Handbook of Photovoltaic Science and Engineering*. John Wiley & Sons, 2011.

[12] Tom Markvart and Luis Castañer, editors. *Practical Handbook of Photovoltaics: Fundamentals and Applications*. Elsevier Ltd, 2003.

[13] Kashif Ishaque, Zainal Salam, and Hamed Taheri. Simple, fast and accurate two-diode model for photovoltaic modules. *Solar Energy Materials and Solar Cells*, 95(2):586–594, 2011.

[14] Jieming Ma, Ka Lok Man, T. O. Ting, Nan Zhang, Sheng-Uei Guan, Prudence W. H. Wong, Jieming Ma, Ka Lok Man, T. O. Ting, Nan Zhang, Sheng-Uei Guan, and Prudence W. H. Wong. Approximate Single-Diode Photovoltaic Model for Efficient I-V Characteristics Estimation. *The Scientific World Journal*, 2013:1–7, 2013.

[15] J.a. Gow and C.D. Manning. Development of a photovoltaic array model for use in power-electronics simulation studies. *IEE Proceedings - Electric Power Applications*, 146(2):193–200, 1999.

[16] Y. Rodríguez-Lazcano, M.T.S. Nair, and P.K. Nair. $CuSbS_2$ thin film formed through annealing chemically deposited Sb_2S_3-CuS thin films. *Journal of Physics D: Applied Physics*, 34(1):12–17, 2001.

[17] Lawrence L. Kazmerski. Solar photovoltaics R&D at the tipping point: A 2005 technology overview. *Journal of Electron Spectroscopy and Related Phenomena*, 150(2-3):105–135, 2006.

[18] Hitoshi Sai, Takuya Matsui, Takashi Koida, Koji Matsubara, Michio Kondo, Shuichiro Sugiyama, Yoshiaki Takeuchi, and Isao Yoshida. Triple-junction thin-film silicon solar cell fabricated on periodically textured substrate with a stabilized efficiency of 13.6%. *Applied Physics Letters*, 106:213902, 2015.

[19] D. L. Staebler and C. R. Wronski. Reversible conductivity changes in discharge-produced amorphous Si. *Applied Physics Letters*, 31(4):292–294, 1977.

[20] R. W. Miles. Photovoltaic solar cells: Choice of materials and production methods. *Vacuum*, 80(10):1090–1097, 2006.

[21] L. El Chaar, L. A. Lamont, and N. El Zein. Review of photovoltaic technologies. *Renewable and Sustainable Energy Reviews*, 15(5):2165–2175, 2011.

[22] First Solar Press Release. First solar achieves yet another cell conversion efficiency world record, 24 February 2016.

[23] Solar Frontier Press Release. Solar Frontier Achieves World Record Thin-Film Solar Cell Efficiency: 22.3%, 8 December 2015. 2015.

[24] NREL. Solar cell efficiency chart, mar 2016.

[25] Wan-Jian Wanjian Yin, Ji-Hui Jihui Yang, Joongoo Kang, Yanfa Yan, and Su-Huai Wei. Halide Perovskite Materials for Solar Cells: A Theoretical Review. *J. Mater. Chem. A*, 3(17):Advance, 2015.

[26] Henry J Snaith. Perovskites : The Emergence of a New Era for Low - Cost , High Efficiency Solar Cells. *Journal of Physical Chemistry Letters*, 4:3623–3630, 2013.

[27] Tze-bin Song, Qi Chen, Huan-Ping Zhou, Chengyang Jiang, Hsin-Hua Wang, Yang Yang, Yongsheng Liu, Jingbi You, and Yang Yang. Perovskite solar cells: film formation and properties. *J. Mater. Chem. A*, 3:9032–9050, 2015.

[28] Zhaoning Song, Suneth C. Watthage, Adam B. Phillips, and Michael J. Heben. Pathways toward high-performance perovskite solar cells: review of recent advances in organo-metal halide perovskites for photovoltaic applications. *Journal of Photonics for Energy*, 6(2):022001, 2016.

[29] Wei Wang, Mark T. Winkler, Oki Gunawan, Tayfun Gokmen, Teodor K. Todorov, Yu Zhu, and David B. Mitzi. Device characteristics of CZTSSe thin-film solar cells with 12.6% efficiency. *Advanced Energy Materials*, 4(7):1–5, 2014.

[30] M P Suryawanshi, G L Agawane, S M Bhosale, S W Shin, P S Patil, J H Kim, and a V Moholkar. CZTS based thin film solar cells: a status review. *Materials Technology: Advanced Performance Materials*, 28(1):98–109, 2013.

[31] C. Garza, S. Shaji, A. Arato, E. Perez Tijerina, G. Alan Castillo, T. K. Das Roy, and B. Krishnan. P-Type $CuSbS_2$ thin films by thermal diffusion of copper into Sb_2S_3. *Solar Energy Materials and Solar Cells*, 95(8):2001–2005, 2011.

[32] D. Colombara, L. M. Peter, K. D. Rogers, J. D. Painter, and S. Roncallo. Formation of CuSbS2 and CuSbSe2 thin films via chalcogenisation of Sb-Cu metal precursors. *Thin Solid Films*, 519(21):7438–7443, 2011.

[33] A Wachtel and A Noreika. Growth and Characterization of $CuSbS_2$ Crystals. *Journal of Electronic Materials*, 9(2):281–297, 1980.

[34] Vijay Kumar Gudelli, V. Kanchana, G. Vaitheeswaran, a. Svane, and N. E. Christensen. Thermoelectric properties of chalcopyrite type $CuGaTe_2$ and chalcostibite $CuSbS_2$. *Journal of Applied Physics*, 114:0–8, 2013.

[35] J W Anthony. *Handbook of Mineralogy: Halides, Hydroxides, Oxides*. Handbook of Mineralogy. Mineral Data Publishing, 1997.

[36] Jesse T R Dufton, Aron Walsh, Pooja M Panchmatia, Laurence M Peter, Diego Colombara, and M Saiful Islam. Structural and electronic properties of

$CuSbS_2$ and $CuBiS_2$: Potential absorber materials for thin-film solar. *Phys. Chem. Chem. Phys.*, 14:7229–7233, 2012.

[37] Satoshi Suehiro, Keisuke Horita, Masayoshi Yuasa, Tooru Tanaka, Katsuhiko Fujita, Yoichi Ishiwata, Kengo Shimanoe, and Tetsuya Kida. Synthesis of Copper-Antimony-Sulfide Nanocrystals for Solution-Processed Solar Cells. *Inorganic chemistry*, pages 2–7, 2015.

[38] C. Tablero. Electronic property analysis of O-doped Cu_3SbS_3. *Solar Energy Materials and Solar Cells*, 104:180–184, 2012.

[39] Bo Yang, Liang Wang, Jun Han, Ying Zhou, Huaibing Song, Shiyou Chen, Jie Zhong, Lu Lv, Dongmei Niu, and Jiang Tang. $CuSbS_2$ as a promising earth-abundant photovoltaic absorber material: A combined theoretical and experimental study. *Chemistry of Materials*, 26:3135–3143, 2014.

[40] B. Krishnan, S. Shaji, and R. Ernesto Ornelas. Progress in development of copper antimony sulfide thin films as an alternative material for solar energy harvesting. *Journal of Materials Science: Materials in Electronics*, 26:4770–4781, 2015.

[41] Mukesh Kumar and Clas Persson. CuSbS2 and CuBiS2 as potential absorber materials for thin-film solar cells. *Journal of Renewable and Sustainable Energy*, 5(3), 2013.

[42] a. Rabhi, M. Kanzari, and B. Rezig. Growth and vacuum post-annealing effect on the properties of the new absorber $CuSbS_2$ thin films. *Materials Letters*, 62(20):3576–3578, 2008.

[43] a. Rabhi, M. Kanzari, and B. Rezig. Optical and structural properties of $CuSbS_2$ thin films grown by thermal evaporation method. *Thin Solid Films*, 517(7):2477–2480, 2009.

[44] a Rabhi and M Kanzari. Effect of air annealing on $CuSbS_2$ thin film grown by vacuum thermal evaporation. *Chalcogenide Letters*, 8(4):255–262, 2011.

[45] Liping Yu, Robert S. Kokenyesi, Douglas a. Keszler, and Alex Zunger. Inverse design of high absorption thin-film photovoltaic materials. *Advanced Energy Materials*, 3:43–48, 2013.

[46] R. E. Ornelas-Acosta, D. Avellaneda, S. Shaji, G. a. Castillo, T. K. Das Roy, and B. Krishnan. $CuSbS_2$ thin films by heating Sb_2S_3/Cu layers for PV applications. *Journal of Materials Science: Materials in Electronics*, 25(10):4356–4362, 2014.

[47] R.E. Ornelas-Acosta, S. Shaji, D. Avellaneda, G.a. Castillo, T.K. Das Roy, and B. Krishnan. Thin films of copper antimony sulfide: A photovoltaic absorber material. *Materials Research Bulletin*, 61:215–225, 2014.

[48] Dainius Perednis. *Thin Film Deposition by Spray Pyrolysis and the Application in Solid Oxide Fuel Cells*. PhD thesis, Swiss Federal Institure of Technology Zurich, 2003.

[49] A. Rabhi and M. Kanzari. Structural, optical, and electrical properties of $CuSbS_2$ these amorphous films: effect of the thickness variation. *Chalcogenide Letters*, 8(6):383–390, 2011.

[50] S C Ezugwu, F I Ezema, and P U Asogwa. Synthesis and characterization of ternary CuSbS2 thin films: effect of deposition time. *Chalcogenide Letters*, 7(5):341–348, 2010.

[51] Y. Fadhli, a. Rabhi, and M. Kanzari. Effect of annealing time and substrates nature on the physical properties of $CuSbS_2$ thin films. *Journal of Materials Science: Materials in Electronics*, 25(11):4767–4773, 2014.

[52] Diego Colombara, Laurence M. Peter, Keith D. Rogers, and Kyle Hutchings. Thermochemical and kinetic aspects of the sulfurization of Cu-Sb and Cu-Bi thin films. *Journal of Solid State Chemistry*, 186:36–46, 2012.

[53] Shigeru Ikeda, Yuta Iga, Wilman Septina, Takashi Harada, and Michio Matsumura. $CuSbS_2$ -based thin film solar cells prepared from electrodeposited

metallic stacks composed of Cu and Sb layers. *Conference Record of the IEEE Photovoltaic Specialists Conference*, pages 2598–2601, 2013.

[54] Wilman Septina, Shigeru Ikeda, Yuta Iga, Takashi Harada, and Michio Matsumura. Thin film solar cell based on $CuSbS_2$ absorber fabricated from an electrochemically deposited metal stack, 2013.

[55] a. C. Rastogi and N. R. Janardhana. Properties of $CuSbS_2$ thin films electrodeposited from ionic liquids as p-type absorber for photovoltaic solar cells. *Thin Solid Films*, 565:285–292, 2014.

[56] Simona Manolache, Anca Duta, Luminita Isac, Marian Nanu, Albert Goossens, and Joop Schoonman. The influence of the precursor concentration on $CuSbS_2$ thin films deposited from aqueous solutions. *Thin Solid Films*, 515(15 SPEC. ISS.):5957–5960, 2007.

[57] S. a. Manolache, L. Andronic, a. Duta, and a. Enesca. The influence of the deposition condition on crystal growth and on the band gap of $CuSbS_2$ thin film absorber used for Solid State Solar Cells (SSSC). *Journal of Optoelectronics and Advanced Materials*, 9(5):1269–1272, 2007.

[58] S a Manolache and A Duta. The influence of the spray deposition parameters in the photovoltaic response of the three-dimensional (M) solar cell: TCO/dense TiO_2/$CuSbS_2$/graphite. *Journal of Optoelectronics and Advanced Materials*, 9(10):3219–3222, 2007.

[59] Ionut Popovici and Anca Duta. Tailoring the Composition and Properties of Sprayed $CuSbS_2$ Thin Films by Using Polymeric Additives. *International Journal of Photoenergy*, 2012:1–6, 2012.

[60] S. Thiruvenkadam and A. Leo Rajesh. Effect of Temperature on Structural and Optical Properties of Spray Pyrolysed $CuSbS_2$ Thin Films for Photovoltaic Applications. *International Journal of Scientific & Technology Research*, 5(1):248–251, 2014.

[61] S Thiruvenkadam and a Leo Rajesh. Effect Of Antimony Concentration On The Properties Of Spray Pyrolysed $CuSbS_2$ Thin Film Absorbing Layer For Photovoltaic Application. *International Journal of Scientific & Technology Research*, 3(2):38–41, 2014.

[62] R. R. Chamberlin and J. S. Skarman. Chemical Spray Deposition Process for Inorganic Films. *Journal of the Electrochemical Society*, 113(1):86–89, 1966.

[63] J C Vigui and J Spitz. Chemical Vapor Deposition at Low Temperatures. *J. Electrochem. Soc.: Solid-State Science and Technology*, 122(4):585–588, 1975.

[64] Dainius Perednis and Ludwig J Gauckler. Thin Film Deposition Using Spray Pyrolysis. *Journal of Electroceramics*, 14:103–111, 2005.

[65] Pramod S Patil. Versatility of chemical spray pyrolysis technique. *Materials Chemistry and Physics*, 59:185–198, 1999.

[66] http://www.spray.com/cat76/automatic-m/offline/download.pdf.

[67] Xiangying Chen, Zhenghua Wang, Xiong Wang, Rui Zhang, Xinyuan Liu, Wanjuan Lin, and Yitai Qian. Synthesis of novel copper sulfide hollow spheres generated from copper (II)-thiourea complex. *Journal of Crystal Growth*, 263(1-4):570–574, 2004.

[68] Chalcogenide Letters, S C Ezugwu, F I Ezema, and P U Asogwa. Synthesis and characterization of ternary $CuSbS_2$ thin films: effect of deposition time. *Chalcogenide Letters*, 7(5):341–348, 2010.

[69] Kirtiman Deo Malviya, Hen Dotan, Ki Ro Yoon, Il-Doo Kima, and Avner Rothschild. Rigorous substrate cleaning process for reproducible thin film hematite (α-Fe_2O_3) photoanodes. *Journal of Materials Research*, 31(October):1–23, 2015.

[70] C R Brundle, C A Evans, and S Wilson. *Encyclopedia of Materials Characterization: Surfaces, Interfaces, Thin Films*. Characterization Series. Butterworth-Heinemann, 1992.

[71] J B Mooney and S B Radding. Spray Pyrolysis Processing. *Annual Review of Materials Science*, 12(1):81–101, 1982.

[72] D R Vij. *Handbook of Applied Solid State Spectroscopy*. Springer US, 2007.

[73] P Eaton and P West. *Atomic Force Microscopy*. OUP Oxford, 2010.

[74] N V Joshi. *Photoconductivity: Art: Science & Technology*. Optical Science and Engineering. Taylor & Francis, 1990.

[75] C Kittel. *Introduction to Solid State Physics*. Wiley, 2004.

[76] B G Yacobi. *Semiconductor Materials: An Introduction to Basic Principles*. Microdevices. Springer US, 2006.

[77] P YU and M Cardona. *Fundamentals of Semiconductors: Physics and Materials Properties*. Graduate Texts in Physics. Springer Berlin Heidelberg, 2010.

[78] Armin G. Aberle. Thin-film solar cells. *Thin Solid Films*, 517(17):4706–4710, 2009.

List of Figures

List of Tables